Evaluating VHEE radiotherapy treatment plans for prostate and lung cancer

B. Spek

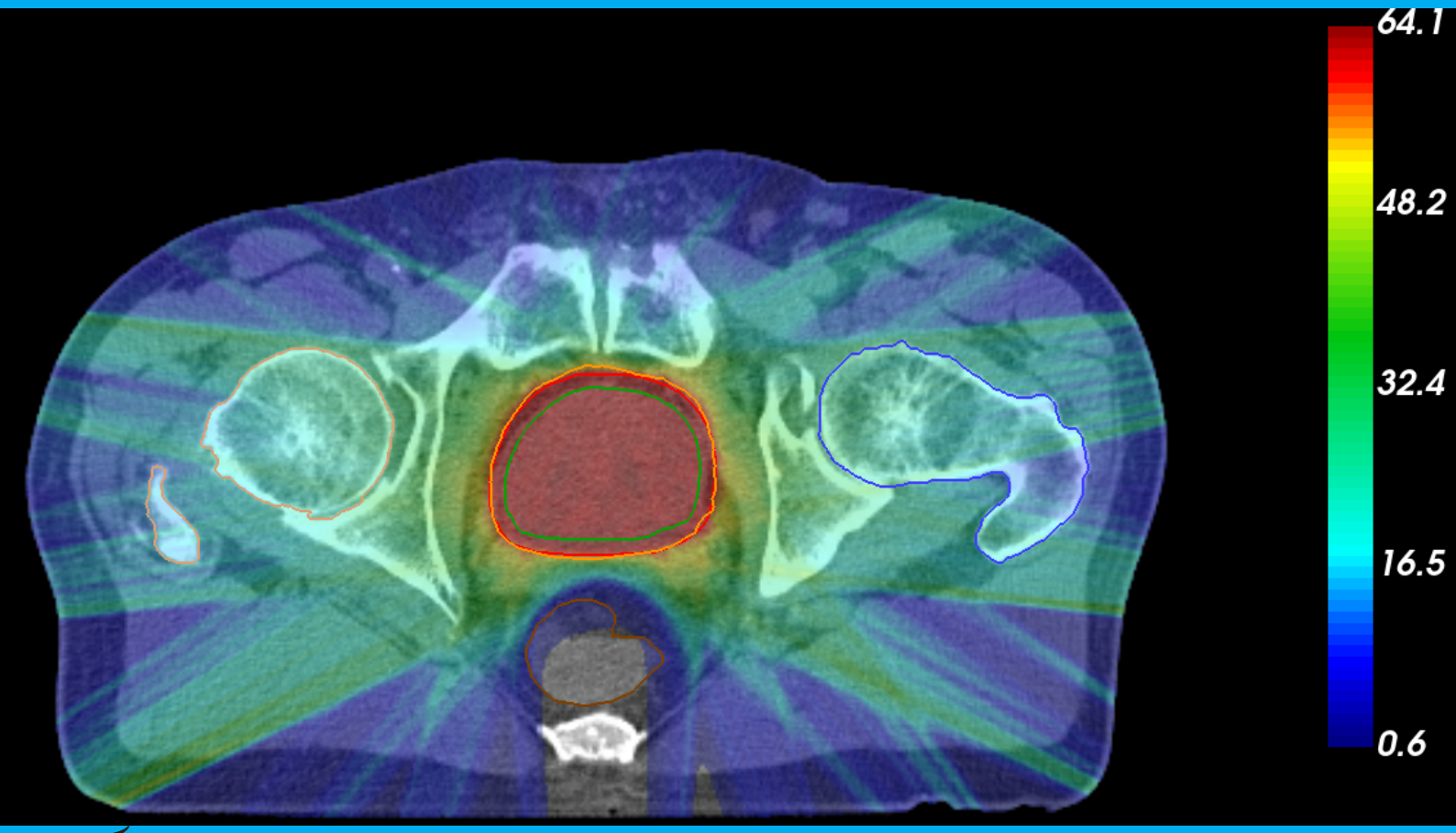

TU Delft

Evaluating VHEE radiotherapy treatment plans for prostate and lung cancer

by

B. Spek

to obtain the degree of Master of Science
at the Delft University of Technology,

Student number: 4951425
Project duration: October 1, 2022 – June 14, 2023
Thesis committee:
Dr. ir. D. Lathouwers, TU Delft, supervisor
Dr. ir. S. Breedveld, ERASMUS MC, supervisor
Dr. ir. A. G. Denkova, TU Delft
Dr. Z. Perkó, TU Delft

An electronic version of this thesis is available at http://repository.tudelft.nl/.

TU Delft

Abstract

Over 50% of cancer patients will receive radiotherapy treatment at least once. Most patients are receiving photon radiotherapy. In this work very high energy electron (VHEE) radiotherapy is being studied as a potential replacement for photon radiotherapy. VHEE beams have a favorable depth dependence and the penumbra of VHEE pencil beams stays small deep inside the patient. Therefore, using VHEE radiotherapy can potentially result in a lower dose being delivered to the organs at risk (OAR) in comparison with clinically used volumetric modulated arc therapy (VMAT). New accelerator techniques allow VHEE beam generators to fit in standard radiotherapy treatment bunkers. Therefore, VHEE therapy can reduce the equipment costs in comparison with proton therapy and it can increase the treatment quality in comparison with photon therapy. In this work the VHEE treatment plans are compared with clinically used VMAT treatment plans for prostate and lung cancer.

VHEE treatment plans were generated for 6 patients with prostate cancer and 3 patients with lung cancer. First, the pencil beam dose distributions were calculated for each patients using a Monte Carlo particle simulation tool called TOPAS MC. Thereafter, the optimal intensities of the pencil beams were calculated using iCycle, an automated optimization tool, which calculates the optimal treatment plan. The VHEE treatment plans are generated with 9, 18 and 36 beams and the energies that are used are: 100, 200, 300 and 400 MeV. The treatment plans were normalized to a 99% PTV coverage of 95% of the prescribed dose.

For the prostate case, the 100 MeV VHEE treatment plans deliver more dose to the organs at risk (OARs) than the VMAT plan. The 18 beam 300 and 400 MeV VHEE treatment plans showed a dose reduction in the mean dose of the patient, the rectum, the anus and the bladder, but a dose increase to the left and right femoral heads. The 18 beam 400 MeV treatment plan reduced the dose to all OARs in comparison with the VMAT plan, for the lung cases. Increasing the number of beams of the VHEE treatment plan reduces the dose to the OARs, for both the prostate and the lung cases. Increasing the energy of the electron beams also reduces the OAR dose for both cases.

VHEE plans reduce the dose to the healthy tissue, while keeping the PTV dose constant and can therefore be considered as a possible replacement for photon radiotherapy.

Contents

1

Introduction

Cancer is among the leading causes of death worldwide. In 2018, there were 18.1 million new cases and 9.5 million cancer-related deaths worldwide. By 2040, the number of new cancer cases is expected to grow to 29.5 million per year, with the number of cancer related deaths increasing to 16.4 million.[1] 12.2% of these cancer incidents are lung cancer and 7.8% are prostate cancer.[2] Patients with cancer can be treated with surgery, chemotherapy or radiotherapy and frequently these modalities are used together. Radiotherapy is one of the main modalities for treating cancer. More than half of all patients with cancer get radiotherapy treatment at least once during their care.[3] Figure 1.1 shows the radiotherapy set-up using a linear accelerator.

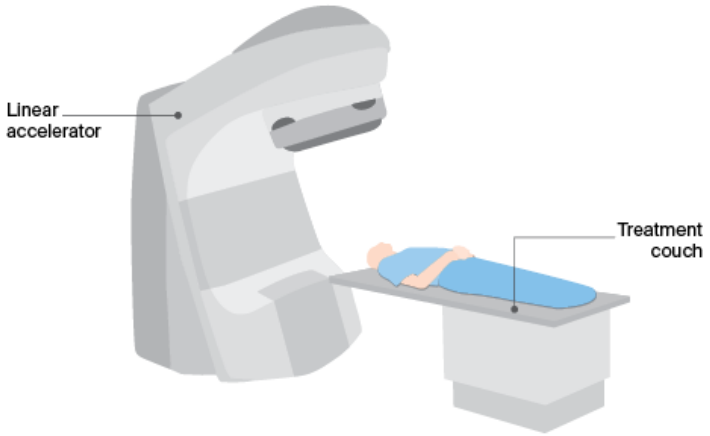

Figure 1.1: Radiotherapy set-up using a linear accelerator.[4]

Most of these patients are treated with photons, with over 15.000 treatment machines for photon radiotherapy worldwide.[5] Other clinical used modalities for external beam radiotherapy are the treatment with electrons, protons or light ions. An important difference between these particles is their percentage depth dose (PDD). This describes the dose distribution over depth. Figure 1.2 shows the PDD for photons, electrons, protons and carbon-12 ions.

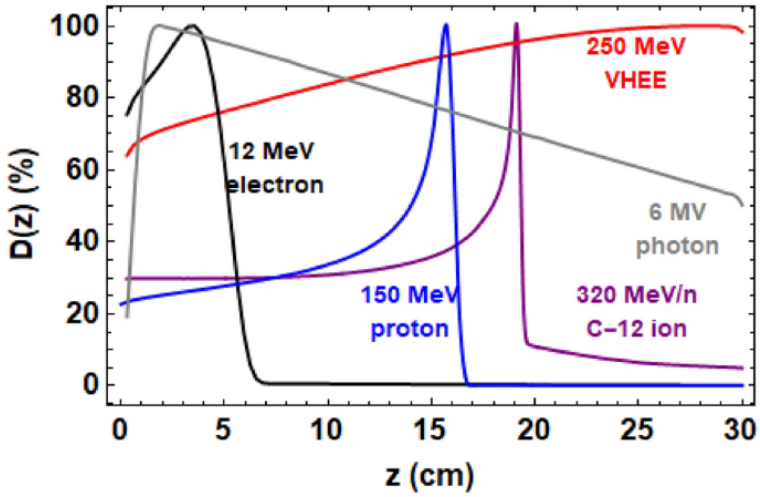

Figure 1.2: Percentage depth dose (PDD) of photons. electrons, protons and carbon-12 ions.[6]

Low energy electrons deposit most of their dose early in the patient and because of that they are used to treat skin cancer.[7] When increasing the energy of the electrons beyond 50 MeV, they have a bigger range and they can reach deep seated tumors. These electrons are called very high energy electrons (VHEE). An advantage of VHEE beams is that they have a very small penumbra. The penumbra is defined as the distance between 80% and 20% dose and it is a measure of how sharp the beam is. The higher the energy of the electron beam, the smaller the penumbra stays in the patient. Photons deliver their dose over a large volume in the patient. Protons and other light ions deliver most of their dose around a specific depth, this dose shape is called the Bragg peak. By changing the energy of the incoming proton beam the peak distance at which most dose is deposited also changes. Therefore, protons can deposit a lot of dose inside the tumor, while sparing the healthy tissue around it. The treatment of cancer with protons has a lot of advantages in comparison with the treatment with photons.[8] However, the biggest downside to proton radiotherapy is that it requires large and expensive equipment.[9] Therefore, this work focuses on VHEE radiotherapy as a cost-effective alternative to proton radiotherapy, while achieving clinically superior treatment plans in comparison with photon therapy. This is done by comparing VHEE radiotherapy treatment plans with VMAT treatment plans for treating prostate cancer and lung cancer.

2

Background Information

2.1. Radiotherapy

The aim of radiotherapy is to kill the tumor cells with the least amount of damage to the healthy tissue to minimize negative side effects of the irradiation. The tumor can be irradiated by implanting radioactive sources inside or next to the tumor (brachytherapy) or with radiation beams from outside the patient (external beam radiotherapy). This report focuses on the latter. External beam radiotherapy was already used in the 1910s for treating skin cancers using X-rays, but still a lot of progress is being made in this field.[10] Radiation beams deposit the highest dose a few cm under the skin, while a tumor generally lies at a depth of 5-20 cm. To mitigate this problem multiple angles are being used to create a cross-fire at the tumor. By using multiple angles the required dose in the tumor volume can be reached while keeping the dose in the healthy tissue low by spreading it out over a large area. The intensity of each beam should be optimized to achieve the best treatment result.

Next to photons, also electrons, protons and carbon ions can be used for radiotherapy treatment.[11] X-ray therapy modalities like intensity modulated radiation therapy (IMRT) and volumetric modulated arc therapy (VMAT) are using a collimator to shape the broad beam as can be seen in Figure 2.1.

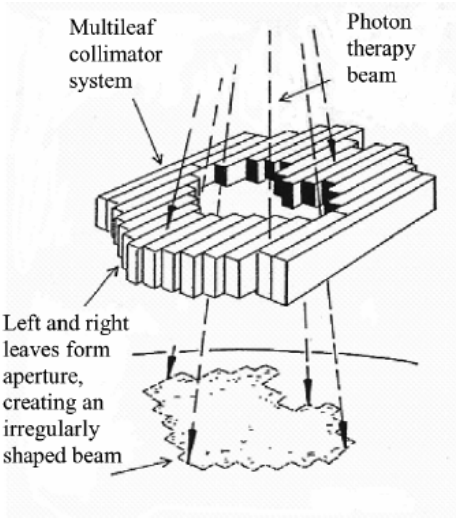

Figure 2.1: A multileaf collimator is used to shape the beam to spare the healthy tissue around the tumor.[12]

When charged particles are being used, pencil beam scanning can be applied. By using pencil beam scanning the pencil beams, narrow beams with diameters to a few millimeter, are deflected by magnets onto a grid. The intensity can be modulated by varying the time a pencil beam is aimed at a certain grid spot. Pencil beam scanning is depicted in Figure 2.2.

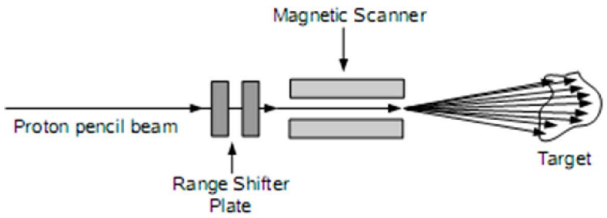

Figure 2.2: A charged particle beam can be scanned over the patient using magnets. Figure from [13]

2.2. Electron interactions

Electrons interact with matter by Coulomb interactions with the nucleus or the orbital electrons of an atom. The electrons can be elastically scattered, they can excite and ionize atoms and they can radiate energy by bremsstrahlung. When electrons interact via elastic scatter the angle of the electron changes and it loses a part of its energy. For high energy electrons this energy loss is a very small part of the initial energy.[14] Furthermore, electrons can excite atoms having inelastic interactions with the orbital electrons. This may cause ionization of the atom in which a secondary electron can be emitted. This process is depicted in Figure 2.3A. It is also possible for electrons to lose energy by radiating bremsstrahlung. This happens when the electron is decelerated in the electric field of an atom due to coulomb forces. The electron loses kinetic energy which is converted into a bremsstrahlung photon. The produced photon spectrum is almost flat for high energy incident electrons.[15] The process of bremsstrahlung is illustrated in Figure 2.3B.

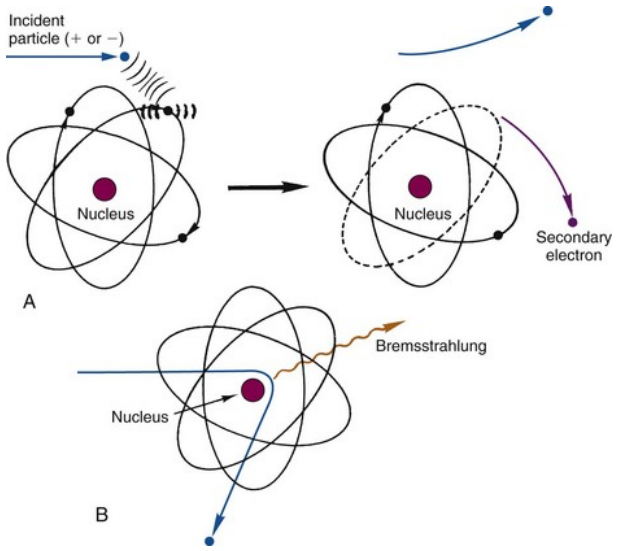

Figure 2.3: Type of interactions of electrons with matter: A shows the excitation and ionization of an atom, B shows the creation of bremsstrahlung.[16]

Electrons lose most of their energy with excitation and ionization of atoms and bremsstrahlung radiation. To compare the energy loss due to the different type of interactions stopping power is used for charged particles, which is the mean energy loss per unit path length. For electrons the term collisional stopping power is used for energy loss by excitation and ionization of atoms and the term radiative stopping power for bremsstrahlung. At 100 MeV these stopping powers are almost identical and for higher energies the radiative stopping power becomes larger as can be seen in Figure 2.4.

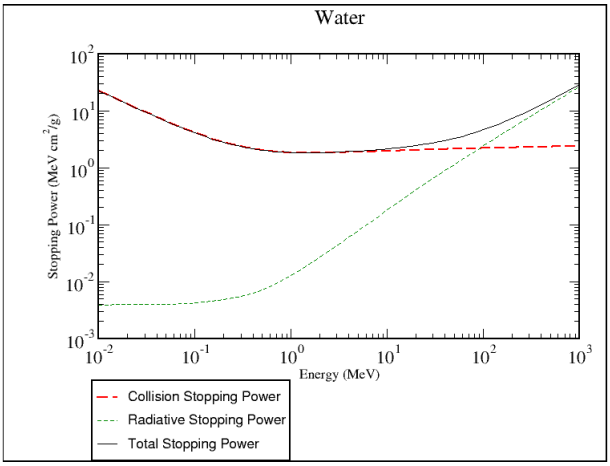

Figure 2.4: Collisional, radiative and total stopping power for electrons in water. [17]

Radiation yield is the average fraction of energy which an electron radiates as bremsstrahlung when slowing down completely. An estimation of the radiation yield Y for electrons with kinetic energy T (in MeV) in water is given by the following formula [18]:

$$Y \approx \frac{4.8 \cdot 10^{-3} T}{1 + 4.8 \cdot 10^{-3} T} \tag{2.1}$$

The radiation yield for 100 MeV electrons is around 0.324 and it increases for higher energy electrons. Because a significant fraction of the energy is released as photons, it is also important to know how photons interact with matter.

2.3. Photon Interactions

The most relevant interactions of photons with matter are the photoelectric effect, Compton scatter and pair production. The interactions are illustrated in Figure 2.5.

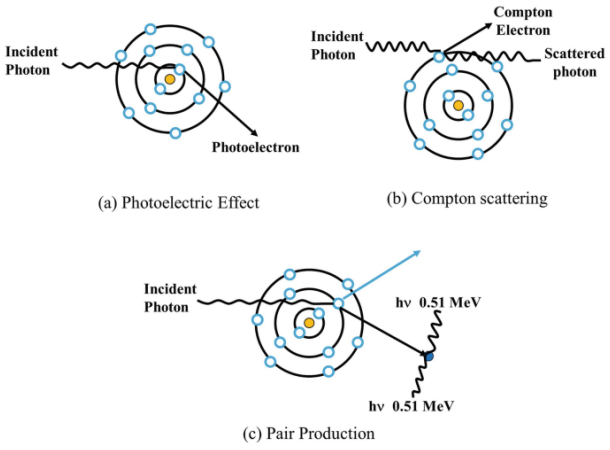

Figure 2.5: The type of interactions photons can have.[19]

The photoelectric effect occurs when a low energy photon gets completely absorbed by an electron and the electron receives more energy than its binding energy. The electron is then emitted by the atom and it is then called a photoelectron. When the photon is not absorbed but only scattered it is called Compton scattering. The emitted electron is then called a Compton electron.

The interaction is called pair production when an electron-positron pair is created by a high energy photon. It can only occur near an atomic nucleus to satisfy conservation of energy and momentum. Pair production is an interaction that only happens with high energy photons, because the photon is

required to have at least the rest energy of the electron and positron combined, which can be calculated using $E = m_e c^2$ giving 1.022 MeV for the total energy a photon needs to have for pair production to be possible. The remaining energy of the photon is transferred into kinetic energy of the produced pair and recoil of the atomic nucleus.

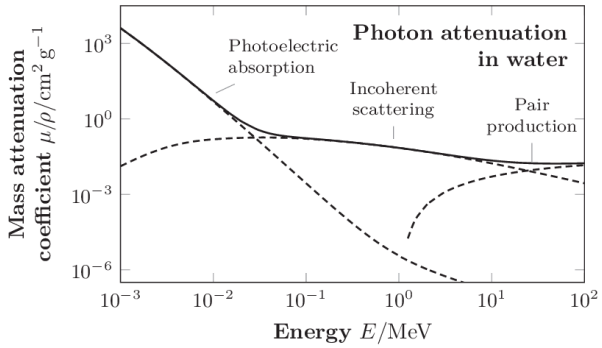

Figure 2.6: Mass attenuation coefficients for photons in water.[20]

In Figure 2.6 the mass attenuation coefficients for photons in water are shown. From this figure, it can be concluded that the dominant interaction types are the photoelectric effect for low energy photons (below 50 keV), Compton scatter for mid range energy photons (between 50 keV and 50 MeV) and pair production for high energy photons (above 50 MeV).

2.4. Tissue response

The tissue response when exposed to radiation is primarily the result of the damage inflicted to DNA.[21] Radiation can cause single and double-strand breaks to the DNA which can result in cell death, malfunctioning of the cell or genetic mutations. Radiation can damage DNA directly, but most damage is done indirectly.[22] Direct damage is caused by ionization of a part of the DNA itself. The indirect damage is caused via radiation-induced hydrolysis of water molecules. The created hydroxyl-radicals (OH) are highly reactive and they damage the DNA structure.[22] Direct and indirect radiation damage is illustrated in Figure 2.7. Currently it is not possible to predict the probability of a specific cell being damaged and being able to repair. Therefore models are used to estimate the macro effects of radiation damage.[23]

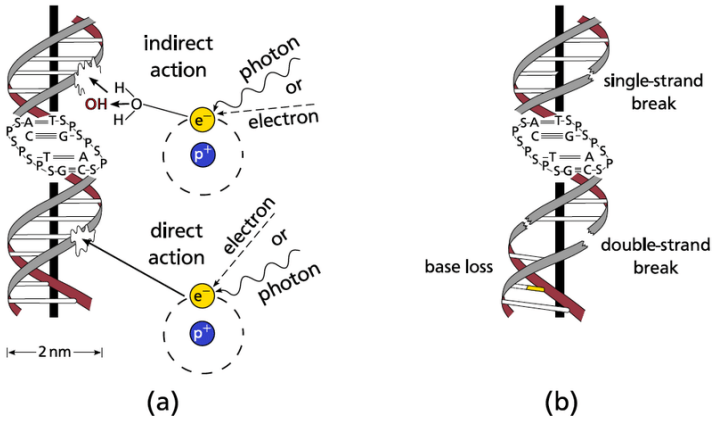

Figure 2.7: (a) Direct and indirect radiation damage to the DNA. (b) Types of radiation damage to the DNA.[22]

The most commonly used model for radiation effects on tissue is the linear-quadratic model.[24] The model was deduced from principles of DNA base pair damage and their repair. The model starts with calculating the surviving fraction of cells,

$$SF_d = e^{-(\alpha d + \beta d^2)}. \tag{2.2}$$

Here d is the dose and α/β determines the sensitivity of tissue for fractionation. Biological effective dose (BED) is then found using

$$SF_d = e^{-\alpha BED}, \tag{2.3}$$

which results in

$$BED = kd * (1 + \frac{d}{\alpha/\beta}). \tag{2.4}$$

k is the number of fractions such that the total dose $D = kd$. α/β values for normal tissue are generally smaller than those for human tumors.[25] Therefore the BED of OARs can be reduced, while keeping the BED for the tumor constant, by increasing the number of fractions k.

The tumor control probability (TCP) is a metric used to define the probability of cure for a patient. To calculate this metric, it is assumed that a patient is cured when there is no detectable or symptomatic tumor left.[26] Using the surviving fraction which was previously mentioned, the TCP can be calculated as follows

$$TCP = e^{-N_0 e^{-k(\alpha d + \beta d^2)}}. \tag{2.5}$$

N_0 is the initial number of malignant cells. In equation 2.5 it is assumed that the number of surviving cells follows a Poisson distribution.[26]

To model the damage to healthy tissue the normal tissue complication probability (NTCP) is used. It gives the probability of a complication to the healthy tissue due to the treatment. The Lyman–Kutcher–Burman (LKB) model is the most well-known NTCP model [27, 28]. In the LKB model, the normal tissue complication probability is calculated as follows:

$$NTCP = \frac{1}{\sqrt{2\pi}} \int_{-\infty}^{t} e^{-\frac{x^2}{2}} dx \tag{2.6}$$

where

$$t = \frac{gEUD - TD_{50}}{m \cdot TD_{50}} \tag{2.7}$$

and

$$gEUD = (\sum_j v_j D_j^{1/n})^n. \tag{2.8}$$

The gEUD is the generalized equivalent uniform dose. TD_{50}, m and n are organ specific parameters and v_j is the fraction of an organ that gets dose D_j. TD_{50} is the tolerance dose for 50 % complication, m is a fit parameter for the steepness of the NTCP curve and n is the volume effect of an organ.

In Figure 2.8, the tumor control probability and the normal tissue complication probability are shown. It is desirable to have a very high TCP, while having a low NTCP. The range where the tumor control probability is much higher than the normal tissue complication probability is called the therapeutic window.

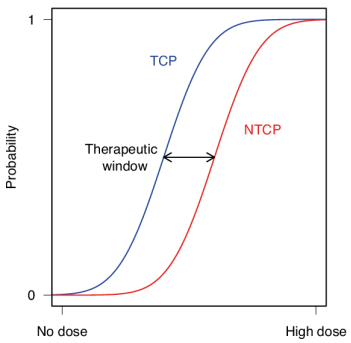

Figure 2.8: The range where the tumor control probability is significantly higher than the normal tissue complication probability is called the therapeutic window. [29]

2.5. VHEE beam generation

Currently electron beams are mainly used for treating skin and superficial tumors. The beam energy used for this type of treatment is between 5 and 20 MeV. Those electron beams are mostly created by linear accelerators.[30] To create very high energy electron beams (>50 MeV) in a clinical setting high gradient accelerators (>100 MeV/m) are needed. Multiple research projects are already performed to acquire such a gradient using linear accelerators.[31, 32, 33]

A promising new method is the use laser wake-field acceleration (LWFA). In this method VHEE beams are created through the interaction of a high power laser pulse with a gaseous target. The laser pulse ionizes the gas and it creates a plasma in which a strong electrostatic gradient (100 GV/m) is being formed. Using this principle a LWFA can accelerate electrons up to the energy required for VHEE in an accelerating region of a few millimeters.[34]

It is very important to take into account the pencil beam parameters, in order to be able to use the VHEE beams in radiotherapy. Not only the energy of the pencil beams, but also the energy spread, the spot size and the divergence of the beams are important. The aim is to use a narrow pencil beam with a low energy spread, such that the treatment plans could be as best as possible. The following values have been found for these parameters. Energy spread = 0.5%, spot size = 2.3 mm x 2.2 mm (FWHM) and divergence = 0.3 mrad.[35, 36, 37, 38]

2.6. Dose distribution VHEE beams

In this section the dose distribution of electron beams will be investigated. Especially the energy dependency of electron beams dose distribution will be depicted.

2.6.1. Depth dose distribution

To show the depth dose distribution the percentage depth dose (PDD) is used. In Figure 2.9 the on-axis PDD and the integrated PDD are shown for 2.5 MeV photons and for 15 and 150 MeV electrons. The integrated PDD is the total dose deposited on a certain depth, while the on-axis PDD is the dose on the central axis of the beam. The difference between the integrated and the on-axis PDD is due to particles scattering away from the central axis. This difference is larger for electrons because they have a higher scatter probability.

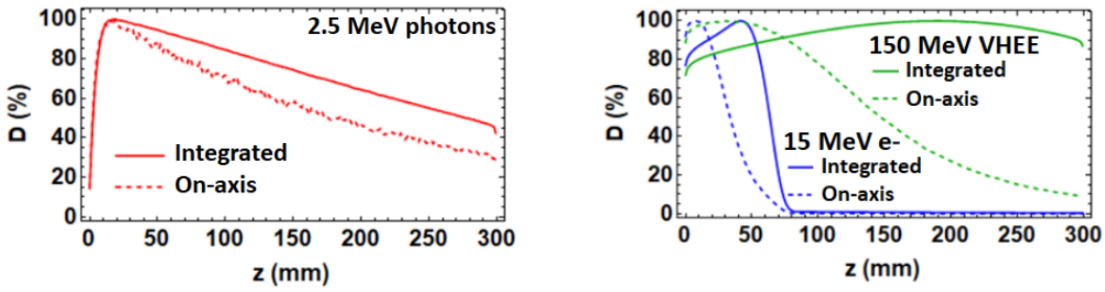

(a) (b)

Figure 2.9: Integrated and on-axis depth dose distribution of 2.5 MeV photons (a) and of 15 and 150 MeV electrons (b) in water.[39]

The depth range of the electron beam is higher for higher energy electrons as can be seen in 2.9(a) for 15 and 150 MeV electron beams. For higher energy electron beams this remains the case which is depicted in Figure 2.10.

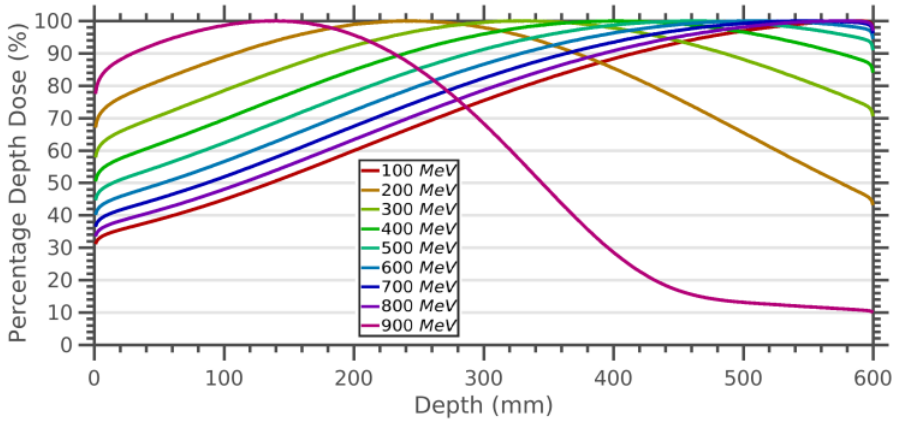

Figure 2.10: Integrated depth dose for VHEE beams 100-900 MeV.[40]

2.6.2. Lateral dose distribution

The lateral distribution of beams is depicted as being Gaussian.[41] The beam spread can be described by the standard deviation sigma. Figure 2.11 shows the beam spread of different energy electron beams propagating through water. The higher the energy of the beam, the narrower the beam will stay while propagating.

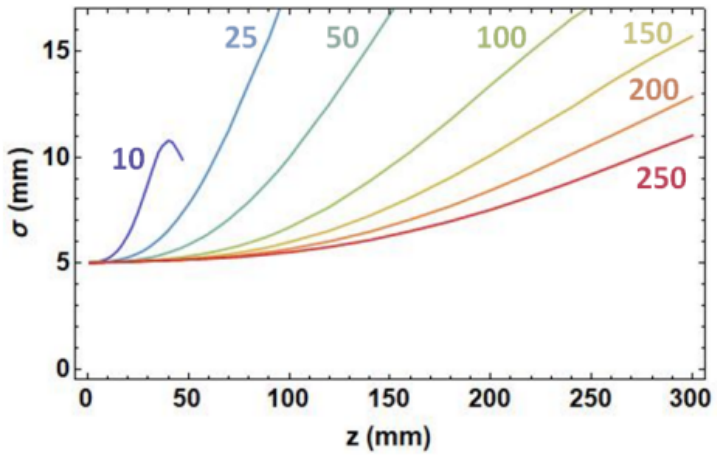

Figure 2.11: Beam spread σ versus depth in water for 10 - 250 MeV (entrance σ = 5 mm for all energies) electron beams.[39]

2.7. Monte Carlo simulation

To calculate the dose distribution in patients the Monte Carlo method is used in this work. The Monte Carlo method uses random sampling to solve mathematical problems. It is a computationally intensive method, but it is seen as the gold standard for dose calculations.[42] Monte Carlo particle transport simulations use cross sections, which give the probability of a certain interaction. Frequently, cross sections are given in barn (b) which is $10^{-28}m^2$.

A Monte Carlo simulation of dose distribution is performed using the following 4 main steps [43]:

1. Random selection of the distance to the next interaction, using the total cross section for the given particle and material properties.

2. Transport the particle to the interaction location taking into account geometry constraints.

3. Selection of the interaction types by random sampling using the partial cross sections.
4. Simulate the selected interaction and production of secondaries, with the resulting particle properties sampled from the corresponding distributions

These four steps are iterated until the primary electron and all the secondaries are either absorbed or escaped from the simulation geometry. A particle is considered absorbed when its energy becomes below a certain threshold. This iterative process is repeated many times to lower the statistical uncertainty of the acquired quantities.

In this report, TOPAS is used [44]. It is a Monte Carlo tool for medical physicist layered on top of the Geant4 code [45]. TOPAS is designed with the goal to make an easy-to-use Monte Carlo simulation tool, such that the users are not required to have an extensive knowledge of the underlying Monte Carlo code. Users only have to generate parameter files that describes the desired simulation. Parameters to specify are: geometry, particle sources, electric or magnetic fields, motion, desired output and physics settings.

2.8. Treatment plan optimization

The quality of a treatment plan depends on the number of beams and their directions. In this report the number of beams and their directions are chosen upfront and the different pencil beams are calculated accordingly. The goal of the optimization is to determine the optimal intensity for each pencil beam in such a way that the dose is minimized in the OARs, while achieving the prescribed dose in the PTV. The dose effect of each pencil beam on the voxels in the patient is calculated prior to the optimization. Then a multi-criteria optimization method is used. Two types of multi-criteria optimizations are in common use in radiotherapy: a posteriori and a priori multi-criteria optimization. In a posteriori multi-criteria optimization, a set of treatment plans is generated, each with a different trade-off between the criteria. This set is then presented to the user (treatment planner), who can interactively explore the trade-offs and select a suitable plan. Disadvantages of the a priori approach are the long computation time, that scales badly with increasing number of criteria, and the difficulty of a human planner to effectively explore a large set of criteria. An alternative approach is developed in Erasmus-iCycle, which uses an a priori multi-criteria approach.[46] The desired trade-offs are automatically defined and results, after a series of optimizations, in a single treatment plan. The configuration is given in a so-called wish-list, comprising treatment constraints, planning goals and their priorities in achieving them. The advantage is that treatment planning can be fully automated and is consistent. Therefore, Erasmus-iCycle is ideal for treatment planning studies, comparing different treatment options for a group of patient cases.

3

Preliminary Analysis

In chapter 2, suitable pencil beam parameters were found. This chapter describes the analysis of several treatment parameters to combine these known pencil beams into a broad beam with acceptable signal-to-noise ratio. First, the distance between the pencil beams will be discussed. Thereafter, the number of histories per pencil beam for the Monte Carlo simulation is determined. In the last section of this chapter, the effect of fiducial markers inside the tumor on the dose distribution is defined.

3.1. Distance between pencil beams

One of the requirements of a good treatment plan is a uniform dose to the tumor volume. In this section the pencil beam spacing needed to achieve this is determined. As mentioned before, the pencil beams will be actively scanned onto a grid in the tumor. Figure 3.1 shows a representation of this grid and the active beam spots with a 2 mm distance between pencil beams.

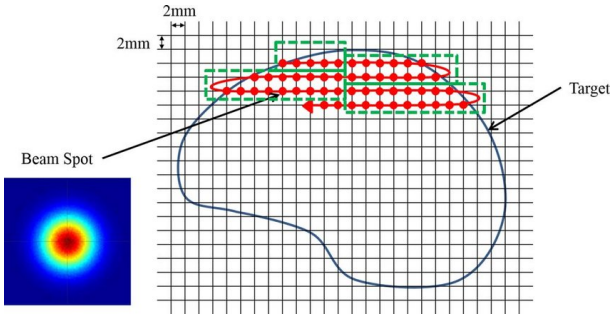

Figure 3.1: Representation of pencil beam scanning grid with 2 mm distance between beam spots. [47]

The 1D cross section of the dose distribution at multiple depths of a 20x20 mm grid of pencil beams in water has been studied for different pencil beam spacings. The pencil beam spacings studied are 1-4 mm for 400 MeV electron pencil beams. The spacing is the same in the x and y direction. Figure 3.2 and 3.3 show the center line dose for 1-4 mm pencil beam distances at multiple depths (with 10^5 particles per pencil beam) for respectively 100 and 400 MeV electron pencil beams. The smaller the spacing, the more uniform the beam becomes but also the more time it takes to compute, because more pencil beams are needed to cover the PTV. To compare the different pencil beam spacings, the difference between the dose on the grid points and the dose exactly in between the grid points is calculated.

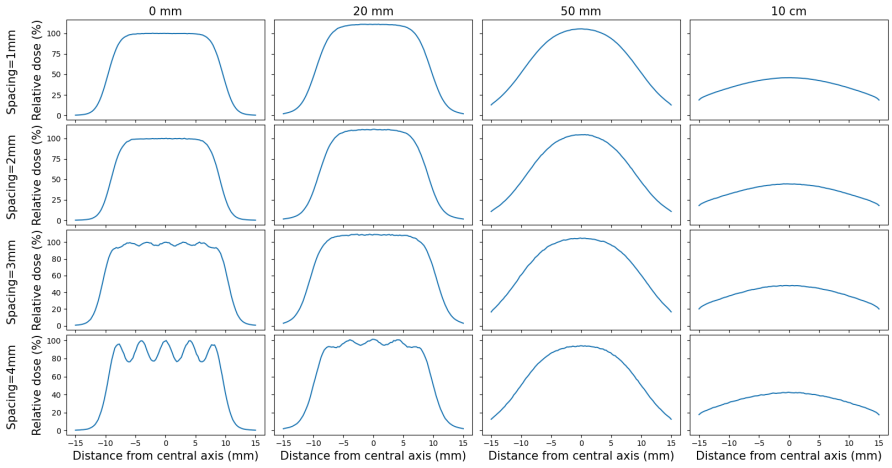

Figure 3.2: 1D center line dose of a 20x20 mm grid of 100 MeV pencil beams in water for multiple spacing at multiple depths.

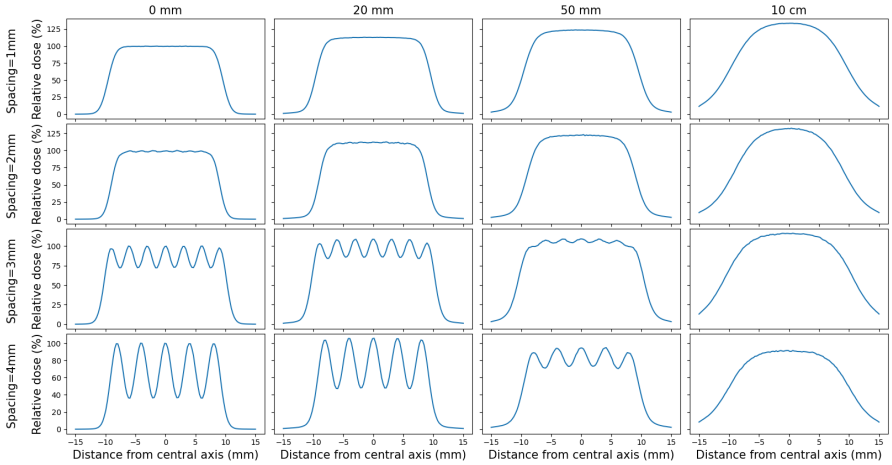

Figure 3.3: 1D center line dose of a 20x20 mm grid of 400 MeV pencil beams in water for multiple spacing at multiple depths.

In Table 3.1 the percentage difference between the dose on the grid points and the dose in between the grid points for the different pencil beam distances is given. The percentages are higher for the 400 MeV energy pencil beams, because higher energy pencil beams have smaller penumbras for a longer distance. Due to scattering, the dose distribution becomes more uniform with higher depths. However the range where it is uniform becomes smaller.

	100 MeV	Depth		400 MeV	Depth	
Spacing	0 mm	20 mm	50 mm	0 mm	20 mm	50 mm
4 mm	24.07%	5.76%	0.71%	62.94%	54.68%	22.49%
3 mm	3.63%	0.76%	0.34%	27.50%	20.91%	3.67%
2 mm	0.69%	0.53%	0.19%	1.09%	0.75%	0.11%
1 mm	0.28%	0.04%	0.005%	0.18%	0.09%	0.12%

Table 3.1: Percentage difference between the dose on the grid points and the dose in between the grid points.

Because in this work deep-seated tumors are treated, the uniformity of the entrance dose is not very important. Therefore the choice is made to use 3 mm spacing between pencil beams. This spacing leads to enough uniformity in the deep-seated tumors, while cutting the computation time by more than half in comparison with a 2 mm spacing.

3.2. Number of histories per pencil beam

An important parameter for Monte Carlo simulations is the number of simulated histories. In general, the larger the number of histories, the more accurate the simulation result becomes, but the more time the computation takes. Theoretically the error reduces with $1/\sqrt{N}$, where N is the number of histories.[48] This means that by doubling the number of histories, the noise reduces by a factor $\sqrt{2}$. The goal in this section is to find the number of histories per pencil beam which results in the optimal trade-off between accuracy and computation time.

The in TOPAS generated pencil beams have the shape of a Gaussian distribution. For beams with large particle densities the scattering behaviour is also Gaussian.[49] Therefore the lateral dose distributions of pencil beams with a different number of histories are compared with a Gaussian function. In Figure 3.4 the lateral dose distribution with the fitted Gaussians are shown for different depths.

To make a choice between the different number of histories for the Monte Carlo simulation, the mean percentage difference between the lateral dose distribution and the Gaussian fit has been calculated. In Table 3.2 the calculated values are stated. Based on these values the choice is made to use 50000 histories per pencil beam for the Monte Carlo simulations.

	Depth		
Number of histories	1.5 cm	6.0 cm	15.0 cm
1000	25.47%	17.88%	61.07%
10000	7.02%	10.50%	21.43%
50000	2.79%	4.64%	11.79%
100000	2.76%	4.36%	9.01%

Table 3.2: Percentage difference between the lateral dose distribution and the Gaussian fit for different number of particles at different depths inside water.

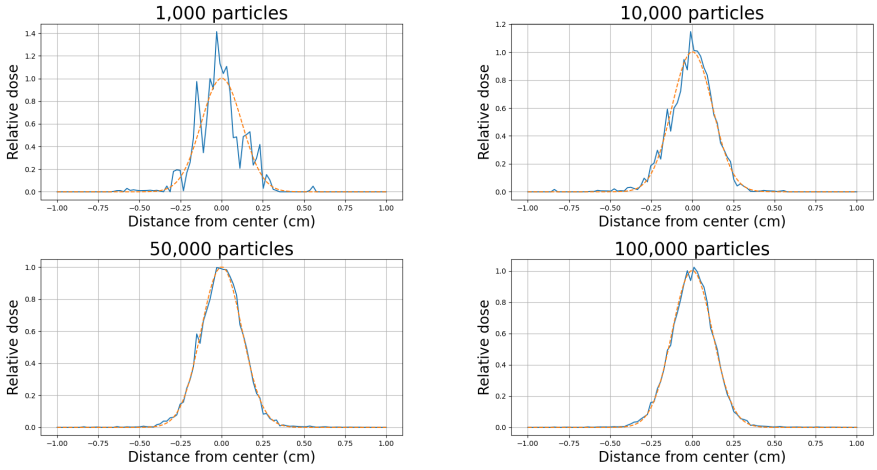

(a)

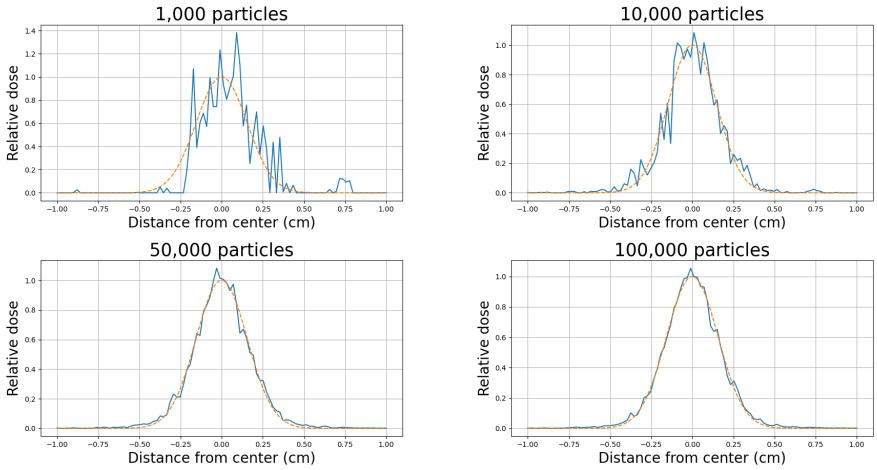

(b)

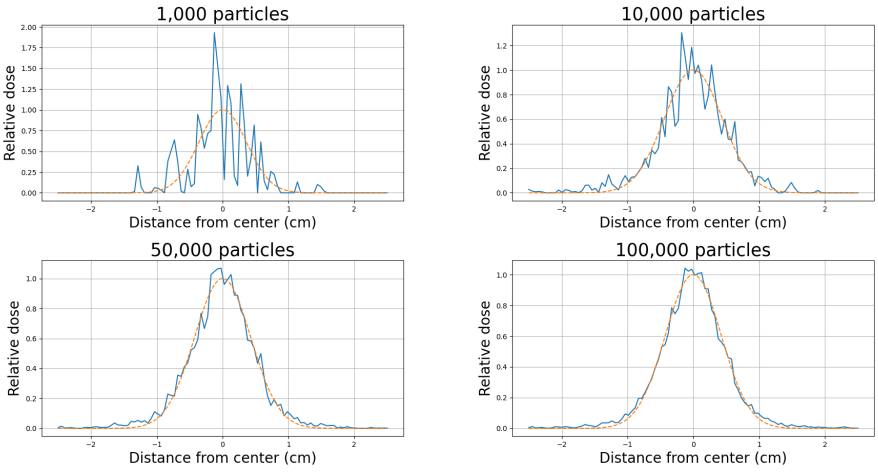

(c)

Figure 3.4: Lateral cross section of a pencil beam at (a) 1.5 cm, (b) 6 cm and (c) 15 cm depth in water. The blue line is the calculated dose and the orange line is a Gaussian fitted on the dose distribution. Made with TOPAS MC using 200 MeV electrons.

3.3. Metal fiducial markers

In radiotherapy, patients are treated over a longer period, daily delivering a fraction of the full treatment. This fractionation is used to increase the therapeutic window, as healthy tissue recovers faster from radiation than malignant tissue. Hereby, sufficient dose to the tumor can be delivered while strongly limiting biological damage to healthy tissues.[50] The exact location of the tumor may be different at the start of each treatment fraction due to prostate motion and patient setup errors. Therefore, image-guided radiotherapy is used for accurate alignment. Frequently, when treating prostate cancer with image-guided radiotherapy, fiducial markers are implanted in the prostate to verify its location.[51] The currently used fiducial markers are mostly made out of metal, because these are well visible on CT scans. They are well visible because the markers have an Hounsfield unit (HU) value up to 3000, while the prostate tissue has a HU value between -100 and 100. Based on the location of the fiducial markers the precise location and orientation of the tumor can be found. Figure 3.5(a) shows a CT slice with two fiducial markers. These metal fiducial markers have a high density and a very high attenuation coefficient in comparison to the prostate tissue.[52] Due to the high attenuation coefficient, the use of markers can result in an undertreated region behind the fiducial markers. Figure 3.5(b) shows the isodose lines of a VHEE beam through the prostate. Behind the markers an undertreated region is created.

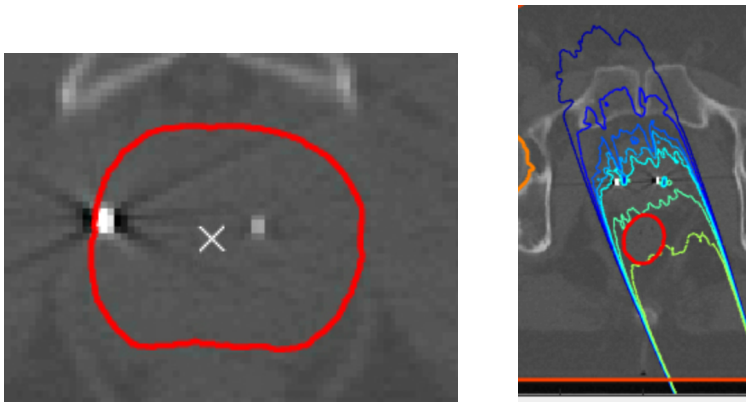

(a) (b)

Figure 3.5: (a) Two metal fiducial markers inside the prostate. (b) 200 MeV electron beam through the prostate, isodose lines are shown. The high attenuation in the metal markers result in a undertreated region behind the markers

The same effect is found when shooting an electron pencil beam through a box of water. Figure 3.6 shows the dose distribution of a 200 MeV electron beam through water with a marker placed at 15 cm depth.

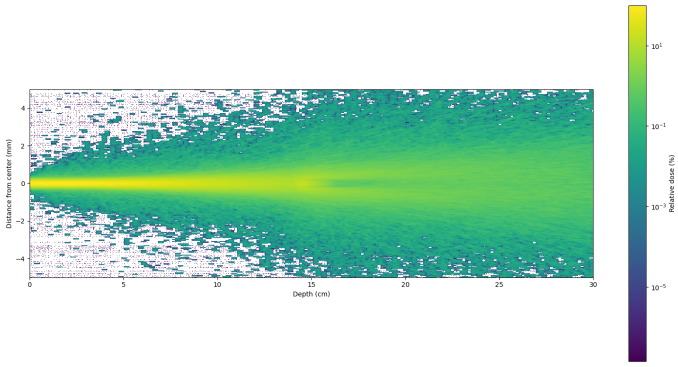

Figure 3.6: 200 MeV electron beam through a water box with a metal fiducial marker placed at 15 cm.

The high attenuation coefficient of the metal marker also causes artefacts on the CT scan. These artefacts are noticable on the CT scan by having a lower density than the tissue around them. Actually, it is the same tissue as around it, but the artefacts are a result of beam hardening. Beam hardening occurs when a beam passes through a very dense material. All the low energy particles are stopped resulting in a beam with an increased mean energy.[53] Another effect of the metal markers is that the beam becomes wider due to an increase in the amount of scattering.[52] Next to that the dose distribution becomes more inhomogeneous due to the metal markers. Not only the metal markers affect the dose distribution of treatment plans, but also the metal artefacts caused by the markers.[54] Regarding clinical practice, also plastic markers with a much lower density could be used. Therefore, in this work the metal markers and their artefacts have been removed from the CT scans before calculating the treatment plan.

To remove the markers and their artefacts the voxels which contain them needs to be selected first. This is done by selecting all the voxels with a HU value that differs from normal prostate tissue. For the markers each voxel with a HU value over 100 is selected and for the artefacts each voxel with a HU value below -30. For each selected voxel the HU value is replaced by the median HU value of the surrounding prostate tissue. The resulting CT slice of this removal is shown in Figure 3.7

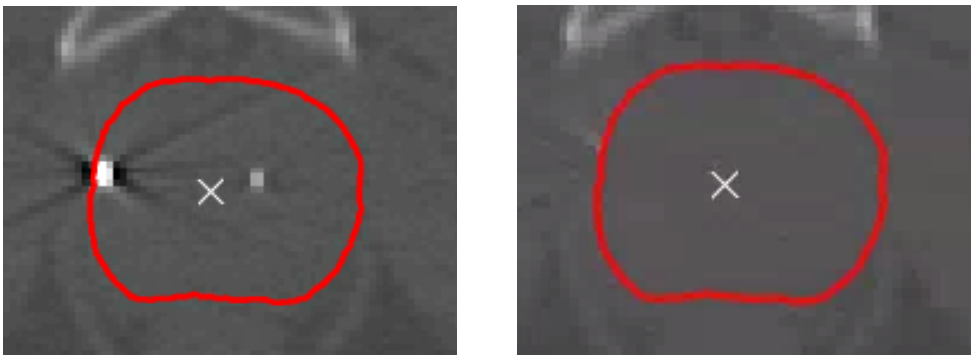

(a) (b)

Figure 3.7: (a) Two metal fiducial markers and artefacts inside the prostate. (b) The prostate with the markers and artefacts removed.

The effect of the marker removal on the dose distribution is shown in Figure 3.8. It shows the same slice of the optimized dose. For Figure 3.8(a) the treatment plan is optimized with the markers and artefacts still on the CT. For Figure 3.8(b) the treatment plan is optimized after the removal of the markers and the artefacts. The removal of the markers and the artefacts results in a more uniform dose in the PTV and around it.

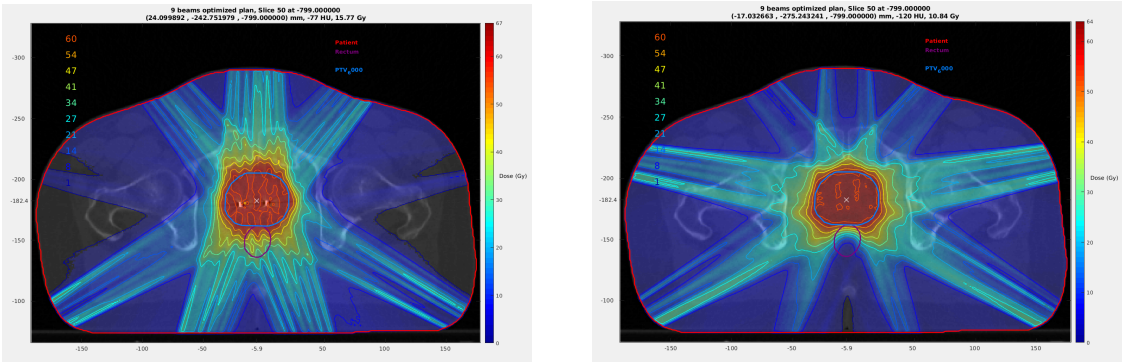

(a) (b)

Figure 3.8: (a) A slice of the dose distribution of the optimized treatment plan for the patient with markers included. (b) A slice of the dose of the optimized treatment plan for the patient with the marker removed.

4

Methods

This chapter describes the methods to generate and evaluate VHEE treatment plans. First the initialization is described. Thereafter, the Monte Carlo simulations and the optimization of the treatment plans is explained. Finally the method to evaluate the treatment plans will be described.

4.1. VHEE initialization

Treatment plans were generated for 6 patients with prostate cancer and 3 patients with lung cancer. For each patient the planning target volume (PTV) and the organs at risk (OAR) where delineated on the CT scan. Also the isocentre of the PTV was determined for each patient based on the CT scans. The isocentre is defined as the point around which the gantry head rotates. For the patients with prostate cancer the fiducial markers and the metal artefacts were removed from the CT scans using the method explained in last chapter. Then all patient data is imported into MATLAB.

Thereafter, the user selects beam angles and beam energy. In this work all the beams are equally distributed over a plane and the only difference is the number of beams used and the energy of these used beams. In this report 9, 18 or 36 beams are used with an energy of 100, 200, 300 or 400 MeV. Figure 4.1 shows an example beam configuration for the treatment of a patient. When the gantry head angles of the beams are known, the scanning angles of the pencil beams are calculated. This is done by overlaying a scanning grid over the PTV. This scanning grid is a Cartesian grid with the prior examined 3 mm spacing between grid points. The x and y scanning angles of each pencil beam are calculated using the distance of each grid point to the isocentre and the source-axis distance (SAD). The SAD is a treatment machine design parameter, but there is no treatment machine for VHEE radiotherapy yet. However, the SAD does only have a small effect on VHEE dose distributions.[55] In this work the SAD is set to 50 cm. After calculation of the scanning angles of the pencil beams they are saved to a MATLAB file together with the gantry head angle of the different beams.

Beam configuration

	Gantry	Couch	Collimator	Isocentre X	Isocentre Y	Isocentre Z	Energy	Algorithm	
1	0	0	0	-11.8	-183.7	-815	200	PB No MLC	VHEE
2	40	0	0	-11.8	-183.7	-815	200	PB No MLC	VHEE
3	80	0	0	-11.8	-183.7	-815	200	PB No MLC	VHEE
4	120	0	0	-11.8	-183.7	-815	200	PB No MLC	VHEE
5	160	0	0	-11.8	-183.7	-815	200	PB No MLC	VHEE
6	200	0	0	-11.8	-183.7	-815	200	PB No MLC	VHEE
7	240	0	0	-11.8	-183.7	-815	200	PB No MLC	VHEE
8	280	0	0	-11.8	-183.7	-815	200	PB No MLC	VHEE
9	320	0	0	-11.8	-183.7	-815	200	PB No MLC	VHEE

Figure 4.1: Beam set-up options. The isocentre is fixed for each patient, so only the gantry head angle and the energy differs between beams.

4.2. Dose calculations using TOPAS

For the dose calculation, TOPAS is used.[44] For the simulations the default physics list is used. The physics list determines which physical processes are taken into account. TOPAS needs all the materials of the patients tissue, however only the Hounsfield unit (HU) values are known from the CT scan. Therefore there needs to be a conversion. The conversion method used was first described by Schneider et al. (2000).[56] He describes the conversion from HU values to tissue parameters. TOPAS uses a conversion file given by the user that contains the element densities for different HU values. In this work, a Python script is used that generates the input files based on the saved MATLAB data about the patient and the beams.

The output of a TOPAS simulation is one 3D dose Dicom file per pencil beam. Because the pencil beams are narrow, a lot of voxels in each Dicom file have a zero dose value. Therefore all the dose data will be saved as sparse matrices. First, all the pencil beam dose files are converted to sparse vectors, by removing all the zero valued voxels and reshape it. Then for each beam, all these pencil beam dose vectors are indexed and combined into a 2D matrix and saved. For the prostate case, the sparse matrices are approximately 1-3 GB of data for each beam, while for the lung case the sparse matrices are around 3-9 GB of data for each beam. This difference is caused by the difference in number of pencil beams per beam for the lung case (around 1200) and for the prostate case (around 500). By sparsifying the dose data, it is compressed with a factor 10.

4.3. iCycle treatment plan optimization

For treatment plan optimization iCycle is used.[46] The optimization algorithm needs the dose distribution data for all used pencil beams. The result of the optimization is a list of intensities for the pencil beams. iCycle uses user created wishlists to calculate the intensities that result in the best possible treatment plan. The wishlist for the optimization of a prostate cancer treatment plan in this thesis is shown in Figure 4.2.

	Structure	Min/Max	Type	Goal	Limit	Sufficient	Priority	Weight	Parameters
1	PTV_6000	Minimize (maximum) ⇩	linear	A*1.05			Constraint	1	
2	Patient	Minimize (maximum) ⇩	linear	A*1.05			Constraint	1	
3	PTV_Shell_50	Minimize (maximum) ⇩	linear	A*0.5			Constraint	1	
4	PTV_6000	Minimize (maximum) ⇩	LTCP	0.7		0.7	1	1	A*0.99 0.9
5	PTV_6000	Minimize (maximum) ⇩	mean	A*1.01			Constraint	1	
6	PTV_Shell_5	Minimize (maximum) ⇩	linear	A*0.85			4	1	
7	PTV_Shell_15	Minimize (maximum) ⇩	linear	0.6*A			6	1	
8	PTV_Shell_25	Minimize (maximum) ⇩	linear	0.3*A			6	1	
9	Rectum	Minimize (maximum) ⇩	linear	58			4	1	
10	Rectum	Minimize (maximum) ⇩	mean	5			5	1	
11	Rectum	Minimize (maximum) ⇩	EUD	30			2	1	12
12	Rectum	Minimize (maximum) ⇩	EUD	20			3	1	8
13	Anus	Minimize (maximum) ⇩	mean	5			5	1	
14	Anus	Minimize (maximum) ⇩	mean	35			Constraint	1	
15	Femur_Head_L	Minimize (maximum) ⇩	linear	40			Constraint	1	
16	Femur_Head_L	Minimize (maximum) ⇩	linear	25			8	1	
17	Femur_Head_R	Minimize (maximum) ⇩	linear	40			Constraint	1	
18	Femur_Head_R	Minimize (maximum) ⇩	linear	25			8	1	
19	Bladder	Minimize (maximum) ⇩	mean	5			7	1	
20	PTV_Shell_10	Minimize (maximum) ⇩	linear	A*0.85			Constraint	1	
21	ExternalRing	Minimize (maximum) ⇩	linear	0.5*A			Constraint	1	

Figure 4.2: A wishlist for the optimization of a prostate cancer treatment plan. A is the prescribed dose parameter.

The wishlist contains objectives and constraints for the different structures of the patient. The structure list includes not only the OARs and the PTV (tumor volume to be irradiated), but also shells around the PTV and the whole patient. The objectives in the wishlist can have a different priority and the priority determines the order at which each objective is optimized. The objectives were optimized by minimizing the maximum dose, the mean dose, the logarithmic tumor control probability (LTCP) or the equivalent uniform dose (EUD) of the selected structure. The optimization consists of two runs. In the first run, if the goal of an objective is reached, the parameter is set to that goal to leave some space for the other objectives to optimize. In the second run, all the objectives that reached the goal in the first run are optimized again to acquire the best possible treatment plan.

4.4. Treatment plan evaluation

Treatment plan evaluation is important to compare different VHEE treatment plans with each other and to compare VHEE treatment plans with the clinically used VMAT treatment plans. All treatment plans will be normalized to a 99% PTV coverage of 95% of the prescribed dose. The first part of the evaluation is done by looking at the dose volume histograms (DVH). A DVH is a graph that shows the percentage of volume of the patient or a specific organ that receives a certain dose. The second part of the evaluation is done by calculating different dose metrics, and calculate if there are statistically significant differences between the treatment plans. This part is only done for the prostate cancer patients. The lung cancer patient group consisted of 3 patients, which was not large enough to properly perform a statistical analysis. The dose metrics evaluated for the prostate cases are shown in Table 4.1.

PTV	Patient	Rectum	Anus	Bladder	Left femoral head	Right femoral head
$V_{95\%}$	D_{mean}	D_{mean}	D_{mean}	D_{mean}	$D_{0.001cc}$	$D_{0.001cc}$
$D_{98\%}$	V_{30Gy}	V_{58Gy}				
$D_{2\%}$	V_{15Gy}	$V_{50\%}$				
D_{mean}	V_{3Gy}					
HI						
$CI_{95\%}$						
CI_{riet}						

Table 4.1: The dose metrics of the different organs, the PTV and the patient to evaluate the treatment plans.

Here $V_{x\%}$ is the relative volume of the structure that receives at least x% of the prescribed dose. $D_{0.001cc}$ gives the maximum dose that is received by at least 0.001 cc of the volume. The dose that is delivered to x% of the volume is given by $D_{x\%}$. Other dose metrics calculated to evaluate the treatment plans are the homogeneity index and the conformity indices. The homogeneity index is calculated with the following formula:

$$HI = \frac{D_{2\%} - D_{98\%}}{D_{50\%}} \tag{4.1}$$

The conformity index $CI_{x\%}$ is the ratio between the volume covered by x% of the reference dose and the volume of the PTV:

$$CI_{x\%} = \frac{V_{x\%}}{V_{PTV}} \tag{4.2}$$

CI_{riet}, another conformity measure, is calculated using the following formula,

$$CI_{riet} = \frac{TV_{RI}}{TV} \cdot \frac{TV_{RI}}{V_{RI}} \tag{4.3}$$

where TV_{RI} is the target volume covered by the reference isodose, TV is the target volume and V_{RI} is the volume of the reference isodose. To compare the treatment plans, T-tests were performed to determine the significance of the difference in dose metric values. Differences were considered statistically significant when the calculated p-value was below 0.05.[57]

5

Results

This chapter reports on the effect of the number of beams and energy of the beams on the VHEE treatment plans. Furthermore, the VHEE treatment plans will be compared with VMAT treatment plans. Finally, the computational performance of the Monte Carlo simulations and the treatment plan optimization will be discussed.

5.1. Prostate cancer patients

5.1.1. Comparing different number of electron beams

In this section the VMAT treatment plans are compared with the VHEE treatment plans for the different number of beams. This is done by showing a slice of the dose distribution in the patient, the population-averaged DVHs for different organs and the PTV and by showing the important dose metrics and calculating if the differences of these metrics are statistically significant.

Figure 5.1 shows a slice of the dose distribution of the VMAT plan and the 300 MeV VHEE plans for different number of beams. The prescribed dose for the prostate cancer patients is 60 Gy. The VMAT plan distributes the dose over a large volume and has a relatively smooth dose profile. The dose profile of the VHEE treatment plans have sharp dose lines as a result of the narrow pencil beams.

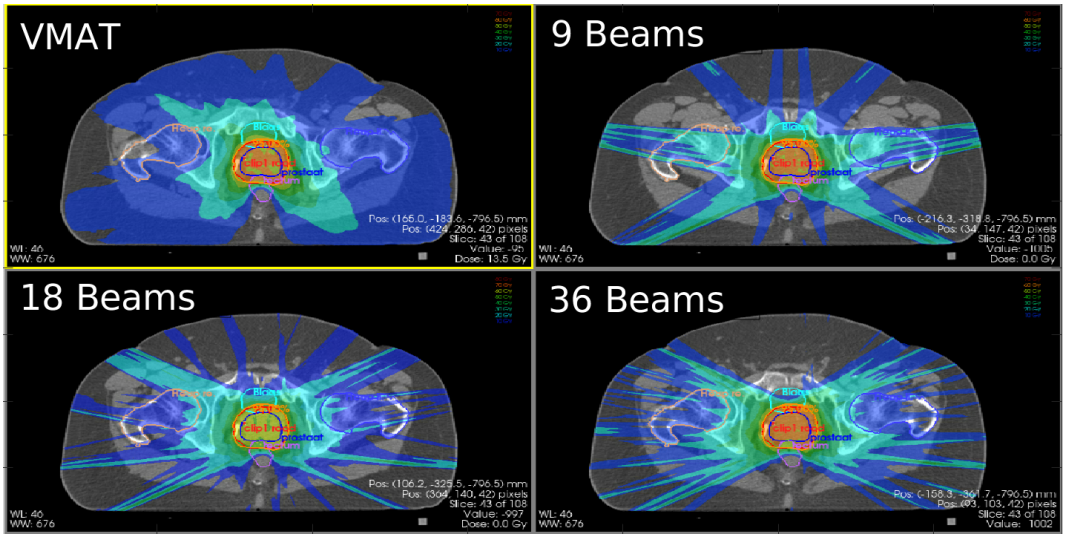

Figure 5.1: Axial slice of the dose distribution for VMAT and VHEE plans with 9,18 and 36 beams with an energy of 300 MeV.

In Figure 5.2, the population averaged DVHs of the PTV, anus, rectum and bladder are shown for VMAT and 100 MeV VHEE treatment plans. For the PTV, the VHEE plans have a sharper DVH than the VMAT plans, but the number of beams does not seem to have an effect. The DVHs of the OARs all look similar. The VMAT treatment plans show lower mean dose in the OAR, but the max dose is higher in comparison with the VHEE plans. For the VHEE treatment plans, the higher the number of beams the lower the mean dose. However, the 36 beam plan still has a higher mean dose than the VMAT plan.

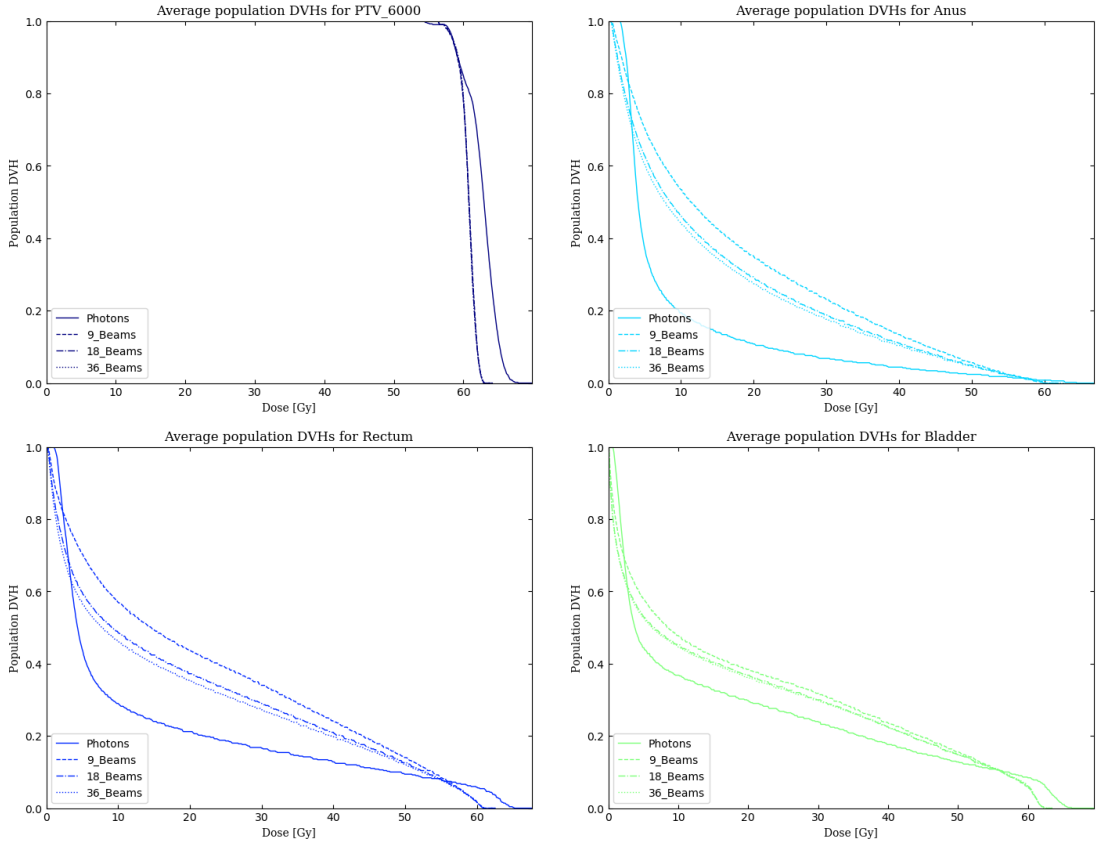

Figure 5.2: Population DVHs of the VMAT treatment plan and the 9, 18, and 36 beams 100 MeV VHEE treatment plans

In Figure 5.3, the population averaged DVHs of the PTV, anus, rectum and bladder are shown for VMAT and 200 MeV VHEE treatment plans. Similar as for the 100 MEV VHEE treatment plans, the DVH of the PTV is sharper for the 200 MeV VHEE plans than for the VMAT plans. For the lower dose levels the volume is higher for the VHEE treatment plans than for the VMAT plans. However, for the anus and the rectum, the VMAT plan still delivers less dose to a large volume, but delivers a higher maximum dose to the organs. For the bladder, the 18 beam VHEE plan has a similar graph as the VMAT plan, while the 36 beam VHEE plan delivers less dose to the bladder than the VMAT plan.

In Figure 5.4, the population averaged DVHs of the PTV, anus, rectum and bladder are shown for VMAT and 300 MeV VHEE treatment plans. Only for the anus the VMAT plans seems preferable over the VHEE plans. The 9 beam VHEE plan results in more dose to the rectum than the VMAT plan, but the 18 and 36 beam VHEE plans reduce the dose to the rectum in comparison with the VMAT plans. For the bladder, all the different VHEE plans result in a decrease in received dose in comparison with the VMAT plans.

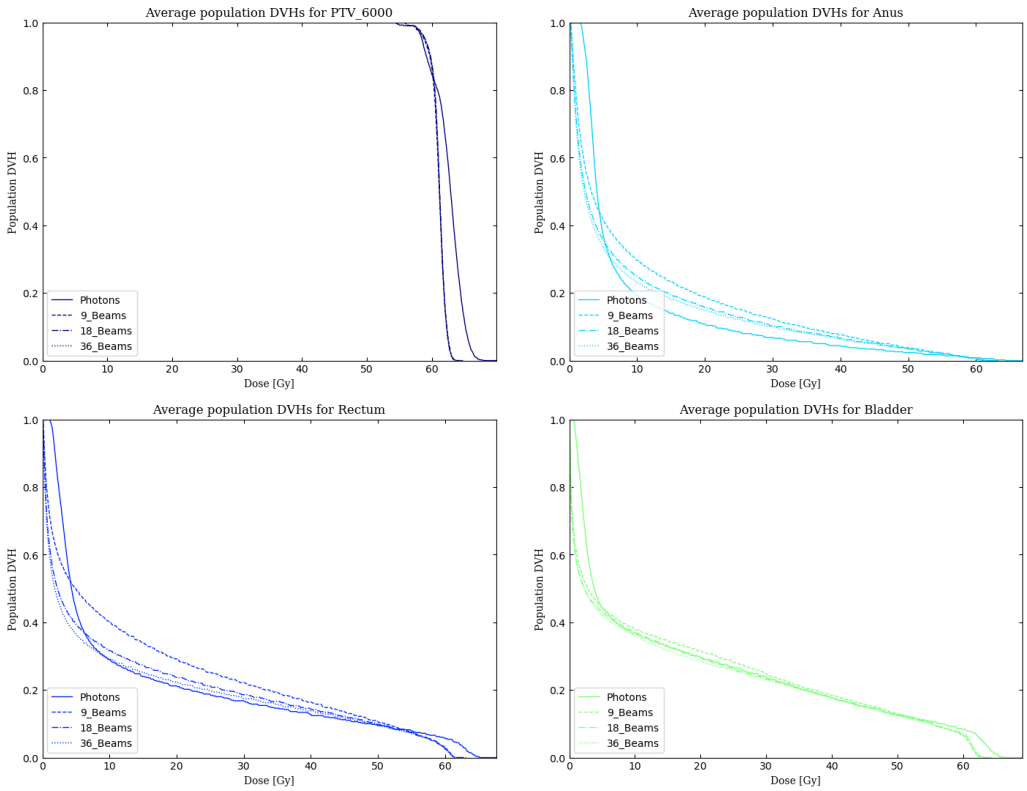

Figure 5.3: Population DVHs of the VMAT treatment plan and the 9, 18, and 36 beams 200 MeV VHEE treatment plans

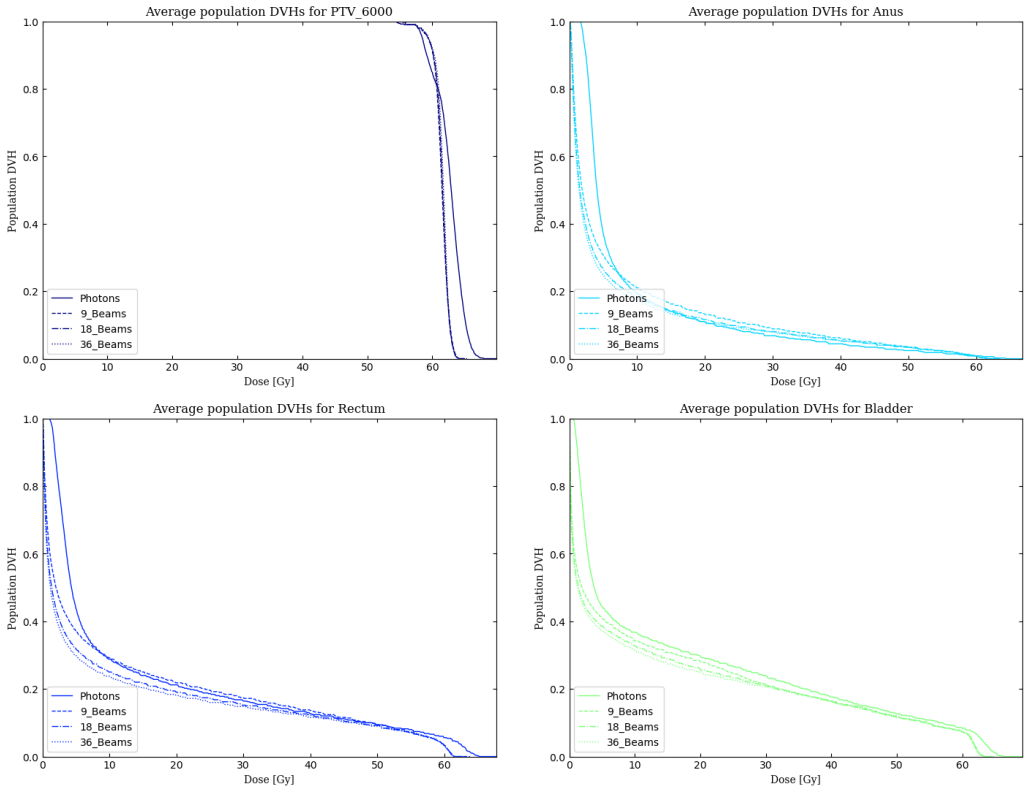

Figure 5.4: Population DVHs of the VMAT treatment plan and the 9, 18, and 36 beams 300 MeV VHEE treatment plans

Figure 5.5 shows the population averaged DVHs of the PTV, anus, rectum and bladder for VMAT and 400 MeV VHEE treatment plans. For the different VHEE treatment plans, the DVH of the PTV differs only slightly from the 36 beam plan. Just like the lower energies, the graph of the PTV is sharper for the VHEE treatment plans. The VHEE plans result in a larger volume of the anus that only receives a small dose, however the volume that receives a higher dose (>25 Gy) is larger for the VHEE plans than for the VMAT plans. For the rectum and the bladder, the 9 beam VHEE plan already reduces the received dose in comparison with the VMAT plans. The 18 and 36 beam plans reduce the delivered dose even further.

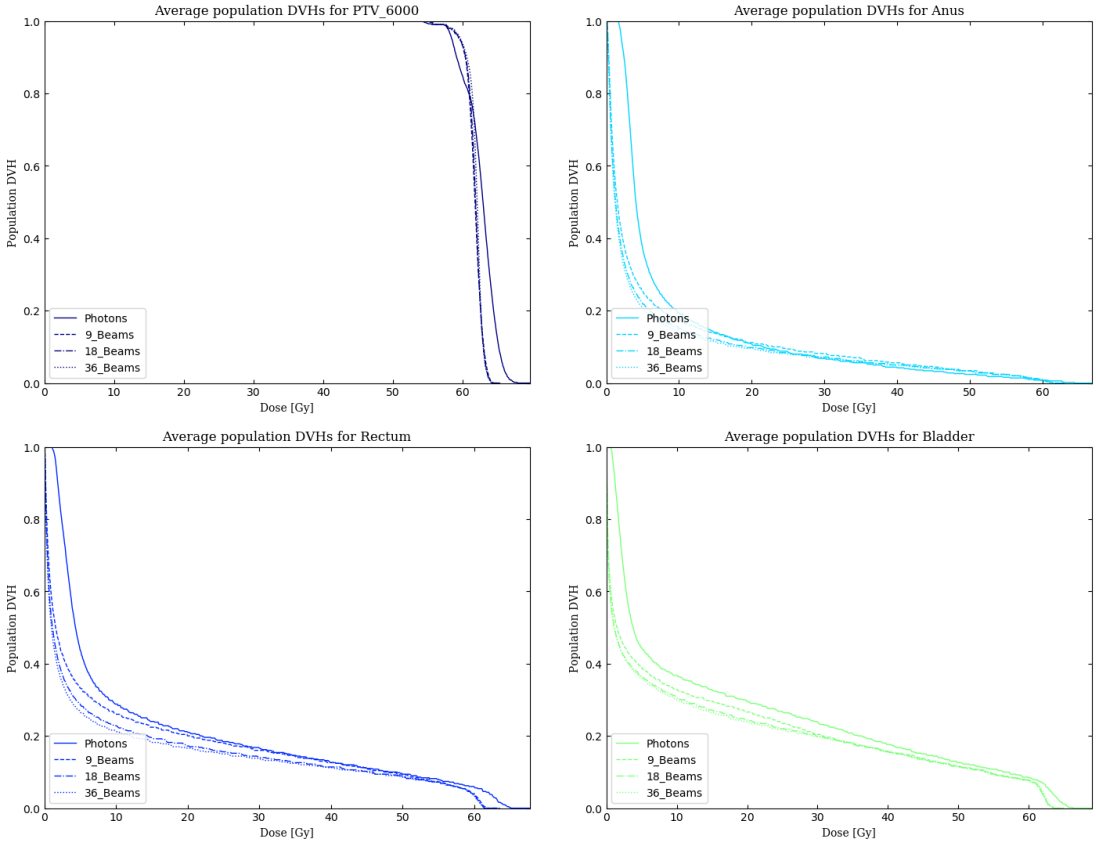

Figure 5.5: Population DVHs of the VMAT treatment plan and the 9, 18, and 36 beams 400 MeV VHEE treatment plans

In Table 5.1 the most relevant dose metrics are shown for the VMAT treatment plans and for the 300 MeV VHEE plans with 9, 18 and 36 beams. Table 5.2 shows the p-values for the differences. The PTV $D_{2\%}$ is significantly reduced from 65.4 Gy to 63.3 Gy, 63.2 Gy and 63.3 Gy for the 9, 18 and 36 beam VHEE plans, respectively. For the 9, 18 and 36 beam VHEE plans the CI_{riet} increases from 0.75 to 0.89, 0.90 and 0.90. The mean dose of the Patient, the rectum, the anus and the bladder are lower for the VHEE treatment plans than for the VMAT plans. These differences are not statistically significant, but this reduction in mean dose was seen for every patient. For the 9 beam VHEE plans, the $D_{0.001cc}$ is significantly higher than for the VMAT plans.

		VMAT	VHEE 9 Beams	VHEE 18 Beams	VHEE 36 Beams
PTV	$V_{95\%}$(%)	98.98 ±0.02	99.00 ±0.01	99.00 ±0.01	99.00 ±0.01
	$D_{98\%}$(Gy)	59.24 ±1.03	58.06 ±0.14	58.13 ±0.10	58.23 ±0.15
	$D_{2\%}$(Gy)	65.44 ±1.99	63.32 ±0.36	63.19 ±0.34	63.26 ±0.43
	D_{mean}(Gy)	62.52 ±1.80	61.34 ±0.30	61.35 ±0.26	61.50 ±0.37
	HI	0.10 ±0.05	0.09 ±0.001	0.08 ±0.002	0.08 ±0.001
	$CI_{95\%}$	0.96 ±0.03	0.93 ±0.04	0.93 ±0.03	0.94 ±0.03
	CI_{riet}	0.75 ±0.03	0.89 ±0.01	0.90 ±0.01	0.90 ±0.01
Patient	D_{mean}(Gy)	4.40 ±0.91	3.51 ±0.70	3.48 ±0.69	3.49 ±0.66
	V_{30Gy}(%)	2.20 ±0.78	2.59 ±0.79	2.33 ±0.77	2.42 ±0.67
	V_{15Gy}(%)	9.82 ±3.43	7.55 ±1.72	7.53 ±1.74	7.50 ±1.70
	V_{3Gy}(%)	24.58 ±3.41	22.71 ±3.53	22.69 ±3.40	22.63 ±3.21
Rectum	D_{mean}(Gy)	13.33 ±4.42	12.14 ±4.63	10.76 ±4.40	10.25 ±4.37
	V_{58Gy}(%)	6.66 ±4.44	5.49 ±3.44	5.51 ±3.47	5.61 ±3.62
	$V_{50\%}$(%)	16.54 ±7.71	17.49 ±7.80	15.40 ±7.43	14.71 ±7.20
Anus	D_{mean}(Gy)	8.55 ±3.91	7.97 ±5.80	7.11 ±5.32	6.80 ±5.27
Bladder	D_{mean}(Gy)	16.28 ±13.44	14.34 ±13.04	13.72 ±12.65	13.39 ±12.70
Left femoral head	$D_{0.001cc}$(Gy)	27.36 ±5.82	38.64 ±4.13	33.21 ±3.78	31.27 ±5.57
Right femoral head	$D_{0.001cc}$(Gy)	28.90 ±5.25	37.51 ±4.40	31.81 ±3.69	32.44 ±3.89

Table 5.1: Dose metrics comparing VMAT with the 9,18 and 36 beams VHEE treatment plans with a beam energy of 300 MeV.

		VMAT - 9 Beams	VMAT - 18 Beams	VMAT - 36 Beams
PTV	$V_{95\%}$	0.081	0.081	0.081
	$D_{98\%}$	0.035	0.043	0.062
	$D_{2\%}$	0.047	0.037	0.044
	D_{mean}	0.186	0.188	0.250
	HI	0.667	0.398	0.397
	$CI_{95\%}$	0.217	0.153	0.323
	CI_{riet}	< 0.001	< 0.001	< 0.001
Patient	D_{mean}	0.121	0.109	0.108
	V_{30Gy}	0.455	0.798	0.645
	V_{15Gy}	0.222	0.220	0.212
	V_{3Gy}	0.419	0.406	0.379
Rectum	D_{mean}	0.689	0.384	0.300
	V_{58Gy}	0.654	0.660	0.693
	$V_{50\%}$	0.851	0.818	0.708
Anus	D_{mean}	0.858	0.639	0.567
Bladder	D_{mean}	0.823	0.764	0.736
Left femoral head	$D_{0.001cc}$	0.008	0.096	0.309
Right femoral head	$D_{0.001cc}$	0.023	0.340	0.260

Table 5.2: p-values of the t-tests between VMAT with the 9,18 and 36 beams VHEE treatment plans with a beam energy of 300 MeV.

5.1.2. Comparing different energies of the electron beams

This section describes the comparison between the VMAT treatment plans and the VHEE treatment plans for different energy electron beams. This is done by showing a slice of the dose distribution in the patient, the population DVHs for different organs and the PTV and by stating the important dose metrics and calculate if the differences of these metrics are statistically significant. The population DVHs of the 100 MeV VHEE treatment plans showed that for each number of beams the dose delivered to the OARs was a lot higher than for the VMAT treatment plans. Therefore, in this section only the 200, 300 and 400 MeV VHEE plans are being shown in the population DVHs.

Figure 5.6 shows a slice of the dose distribution of the VHEE plans with 18 beams for different energy electron beams. The higher the energy of an electron beam the longer the penumbra stays small. Therefore the dose lines are smaller for the higher energy VHEE treatment plans. Another difference that was noticed, is that the higher the energy the more centered the high dose is around the PTV. Especially for the 100 MeV plan the dose is distributed over a larger volume.

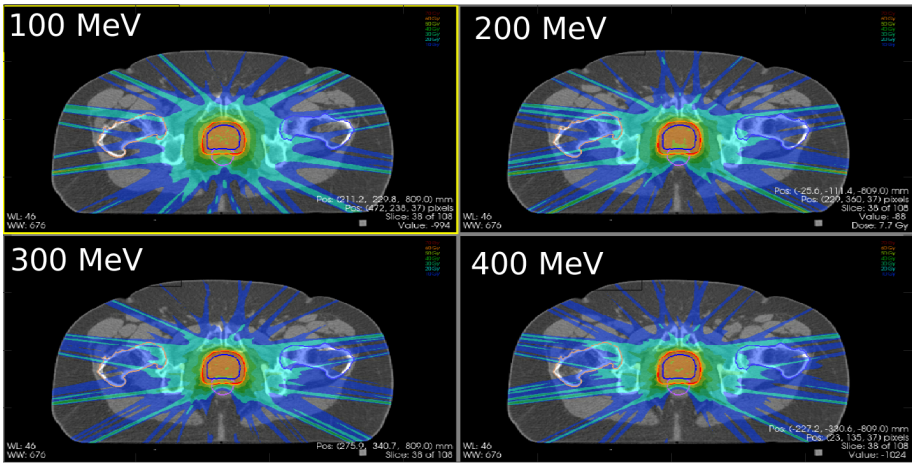

Figure 5.6: Axial slice of the dose distribution of VHEE plans with 18 beams with 100, 200, 300 and 400 MeV electron beams.

Figure 5.7 shows the population averaged DVHs of the PTV, anus, rectum and bladder for the VMAT plans and the 9 beams VHEE treatment plans. The VHEE plan DVHs of the PTV for different beam energies differ more than for the different number of beams. For the anus, the VMAT plan outperforms the VHEE plans. For the rectum, the VMAT plans result in less dose to the organ than the 200 MeV VHEE plans, while the VMAT plans dose to the organ is almost equal than with the 300 and 400 MeV VHEE plans. The 200 MeV plans deliver more dose to the bladder, while the 300 and 400 MeV plans result in a reduction of the dose to the bladder in comparison with the VMAT plans.

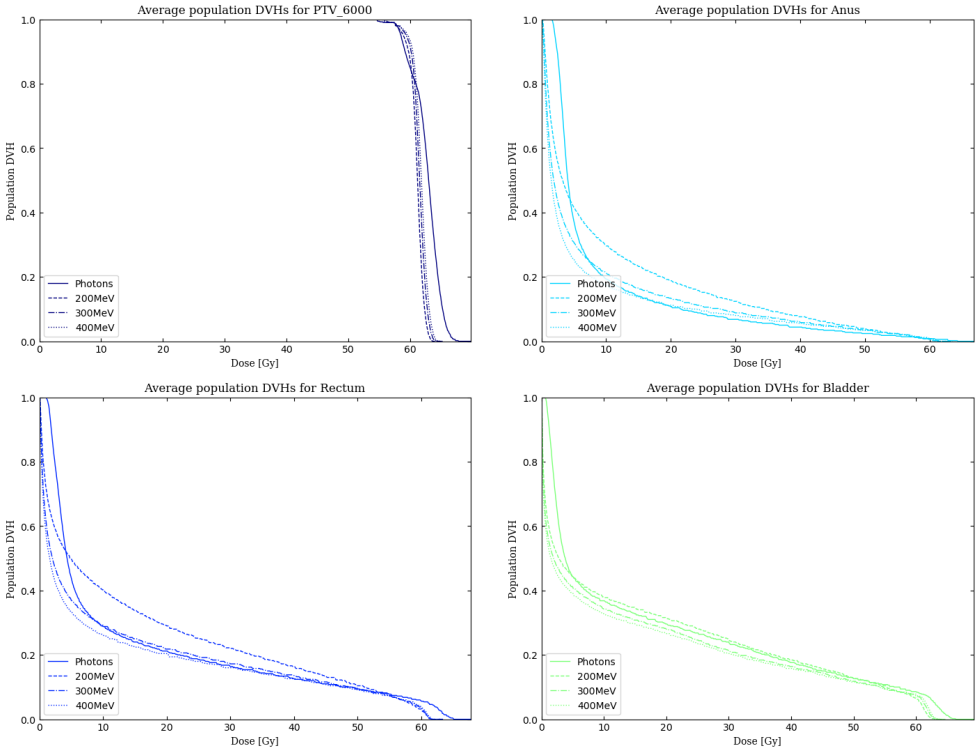

Figure 5.7: Population DVHs of the VMAT treatment plan and the 200,300 and 400 MeV VHEE treatment plans with 9 beams

In Figure 5.8 and 5.9, the population averaged DVHs of the PTV, anus, rectum and bladder are shown for VMAT and 18 and 36 beam VHEE treatment plans, respectively. A difference in comparison with the DVHs of the 9 beam VHEE plans is that for the 18 and 36 beam plans, next to the 400 MeV VHEE plan, also the 300 MeV VHEE plan outperforms the VMAT plans for the rectum. For the bladder, the DVHs of the VMAT plans and the 200 MeV VHEE plans are very similar, but the 300 and 400 MeV VHEE plans deliver less dose to the organ in comparison with the VMAT plans.

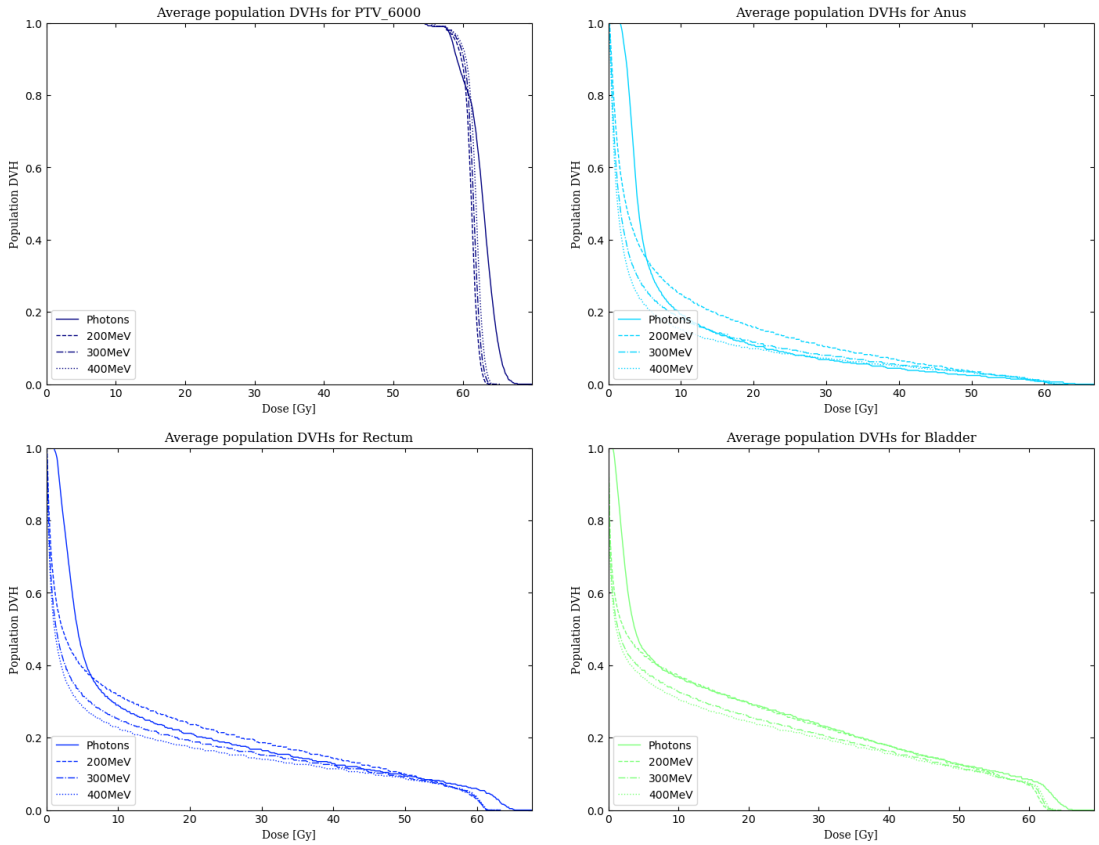

Figure 5.8: Population DVHs of the VMAT treatment plan and the 200,300 and 400 MeV VHEE treatment plans with 18 beams

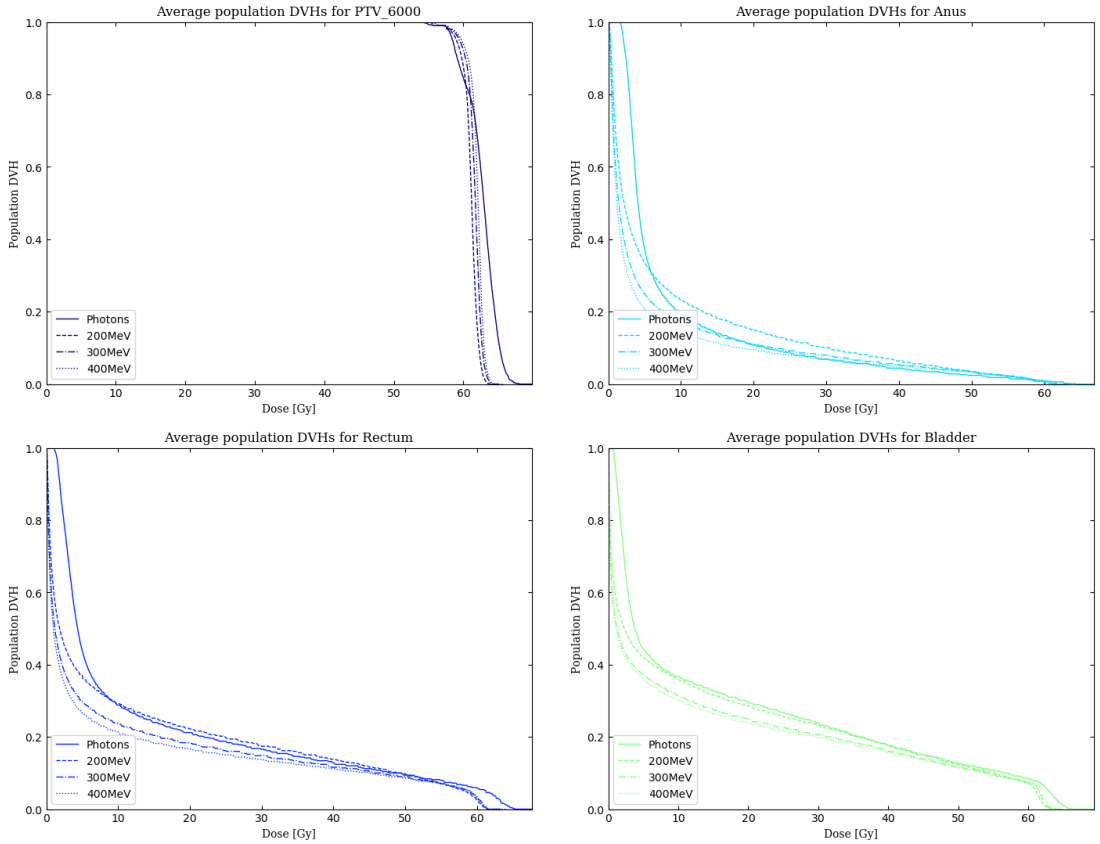

Figure 5.9: Population DVHs of the VMAT treatment plan and the 200,300 and 400 MeV VHEE treatment plans with 36 beams

In Table 5.3 the most relevant dose metrics are shown for the VMAT treatment plans and for the 18 beam VHEE plans with 100, 200, 300 and 400 energy electron beams. Table 5.4 shows the p-values for the differences. The PTV $D_{2\%}$ is significantly reduced from 65.4 Gy to 62.5 Gy, 62.9 Gy and 63.2 Gy for the 100, 200 and 300 MeV VHEE plans, respectively. For the 200, 300 and 400 MeV VHEE plans the CI_{riet} increases from 0.75 to 0.87, 0.90 and 0.91. The mean dose of the patient is lower for all the 18 beam VHEE treatment plans in comparison with the VMAT plans. The mean dose of the anus and Rectum is lower for the VHEE treatment plan with at least 200 MeV beams. The mean dose of the bladder is lower for 300 MeV and 400 MeV VHEE treatment plans. These differences are not statistically significant, but this reduction in mean dose was seen for every patient.

			VHEE			
		VMAT	100 MeV	200 MeV	300 MeV	400 MeV
PTV	$V_{95\%}$(%)	98.98 ±0.02	99.00 ±0.01	99.00 ±0.01	99.01 ±0.03	99.01 ±0.02
	$D_{98\%}$(Gy)	59.24 ±1.03	57.57 ±0.10	57.89 ±0.13	58.15 ±0.16	58.35 ±0.14
	$D_{2\%}$(Gy)	65.44 ±1.99	62.51 ±0.10	62.86 ±0.26	63.20 ±0.38	63.62 ±0.28
	D_{mean}(Gy)	62.52 ±1.80	60.60 ±0.06	61.03 ±0.25	61.37 ±0.30	61.71 ±0.24
	HI	0.10 ±0.05	0.08 ±0.001	0.08 ±0.001	0.08 ±0.002	0.09 ±0.001
	$CI_{95\%}$	0.96 ±0.03	0.83 ±0.03	0.89 ±0.04	0.93 ±0.03	0.96 ±0.02
	CI_{riet}	0.75 ±0.03	0.74 ±0.05	0.87 ±0.01	0.90 ±0.01	0.91 ±0.004
Patient	D_{mean}(Gy)	4.40 ±0.91	3.96 ±0.70	3.56 ±0.67	3.48 ±0.69	3.41 ±0.70
	V_{30Gy}(%)	2.20 ±0.78	2.98 ±0.78	2.47 ±0.87	2.33 ±0.77	2.19 ±0.80
	V_{15Gy}(%)	9.82 ±3.43	9.08 ±1.91	7.70 ±1.62	7.53 ±1.73	7.34 ±1.81
	V_{3Gy}(%)	24.58 ±3.41	22.52 ±2.91	22.89 ±3.17	22.69 ±3.39	22.32 ±3.12
Rectum	D_{mean}(Gy)	13.33 ±4.42	18.89 ±5.40	12.87 ±4.84	10.74 ±4.42	9.90 ±4.05
	V_{58Gy}(%)	6.66 ±4.44	4.66 ±3.13	5.19 ±3.33	5.46 ±3.50	5.64 ±3.55
	$V_{50\%}$(%)	16.54 ±7.71	29.01 ±11.21	18.76 ±8.67	15.40 ±7.49	14.10 ±6.77
Anus	D_{mean}(Gy)	8.55 ±3.91	15.13 ±7.99	9.06 ±6.29	7.11 ±5.31	6.23 ±4.85
Bladder	D_{mean}(Gy)	16.28 ±13.44	18.70 ±14.50	15.15 ±13.83	13.72 ±12.64	13.12 ±12.37
Left femoral head	$D_{0.001cc}$(Gy)	27.36 ±5.82	35.90 ±6.55	33.26 ±6.48	32.90 ±4.31	31.56 ±4.19
Right femoral head	$D_{0.001cc}$(Gy)	28.90 ±5.25	35.04 ±8.66	32.97 ±6.89	31.96 ±3.90	33.32 ±2.28

Table 5.3: Dose metrics comparing VMAT with different energy VHEE treatment plans with 18 beams.

		VMAT - 100 MeV	VMAT - 200 MeV	VMAT - 300 MeV	VMAT - 400 MeV
PTV	$V_{95\%}$	0.081	0.081	0.100	0.045
	$D_{98\%}$	0.007	0.020	0.048	0.092
	$D_{2\%}$	0.011	0.021	0.039	0.077
	D_{mean}	0.044	0.104	0.197	0.348
	HI	0.397	0.397	0.398	0.667
	$CI_{95\%}$	< 0.001	0.014	0.153	1.000
	CI_{riet}	0.711	< 0.001	< 0.001	< 0.001
Patient	D_{mean}	0.416	0.135	0.109	0.090
	V_{30Gy}	0.153	0.619	0.798	0.985
	V_{15Gy}	0.685	0.247	0.219	0.191
	V_{3Gy}	0.334	0.441	0.405	0.306
Rectum	D_{mean}	0.113	0.879	0.381	0.237
	V_{58Gy}	0.434	0.570	0.648	0.699
	$V_{50\%}$	0.075	0.680	0.819	0.609
Anus	D_{mean}	0.137	0.881	0.638	0.429
Bladder	D_{mean}	0.791	0.899	0.764	0.709
Left femoral head	$D_{0.001cc}$	0.061	0.168	0.126	0.227
Right femoral head	$D_{0.001cc}$	0.212	0.324	0.326	0.123

Table 5.4: p-values of the t-tests between VMAT and the four different energy VHEE treatment plans with 18 beams.

5.2. Lung cancer patients

5.2.1. Comparing different number of electron beams

In this section the VMAT treatment plan is compared with the VHEE treatment plans for the different number of beams. This is done by showing a slice of the dose distribution in the patient and showing the DVHs for different organs and the PTV.

Figure 5.10 shows a slice of the dose distribution of the VMAT plan and the 400 MeV VHEE plans for different number of beams. The prescribed dose for the lung cancer patients is 66 Gy.

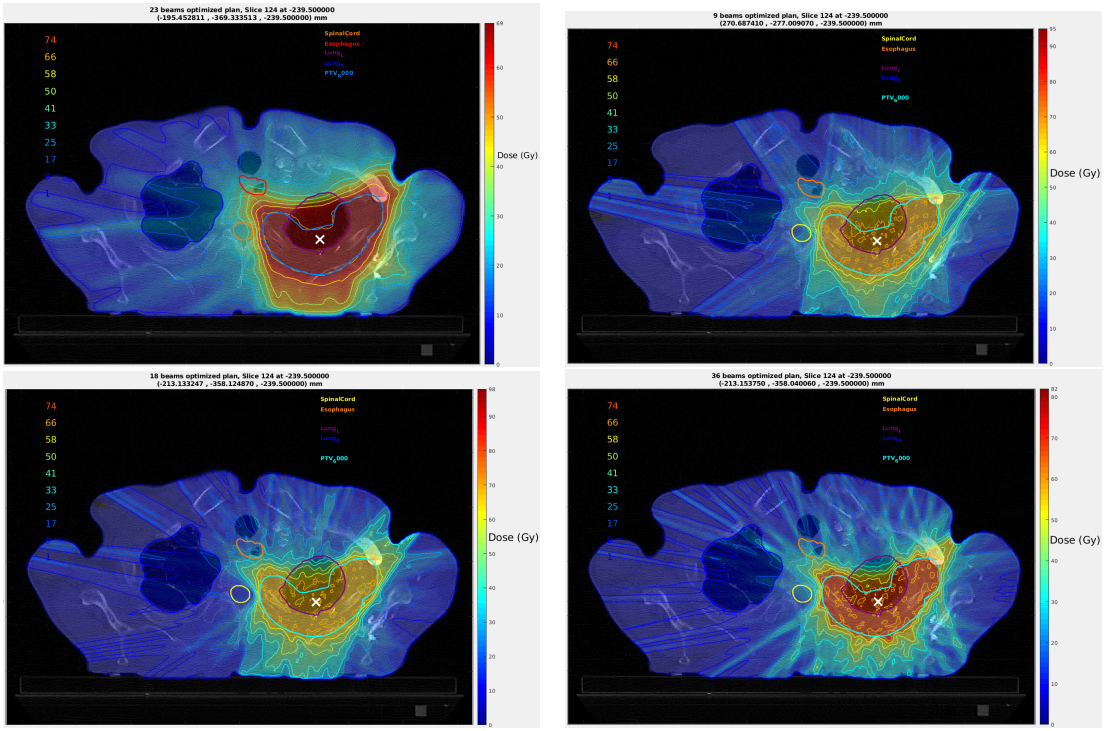

Figure 5.10: Axial slice of the dose distribution for VMAT and VHEE plans with 9,18 and 36 beams with an energy of 400 MeV. Top left is VMAT, top right is 9 beam VHEE, bottom left is 18 beam VHEE and the bottom right is 36 beam VHEE.

In Figure 5.11 the DVHs of the PTV, esophagus, spinal cord and plexus are shown for the VMAT plan and the 400 MeV VHEE plans with 9, 18 and 36 beams. The graph of the PTV is sharper for the VMAT plan than for the VHEE plans. For the esophagus the VHEE treatment plans deliver less dose to the organ than the VMAT plan. Also the higher the number of beams, the lower the delivered dose to the esophagus. The VHEE plans also deliver less dose to the spinal cord than the VMAT plan, but the 18 beam VHEE plan results in less dose to the organ than the 36 beam VHEE plan for the spinal cord. Also for the plexus, the 18 beam VHEE plan results in the lowest dose.

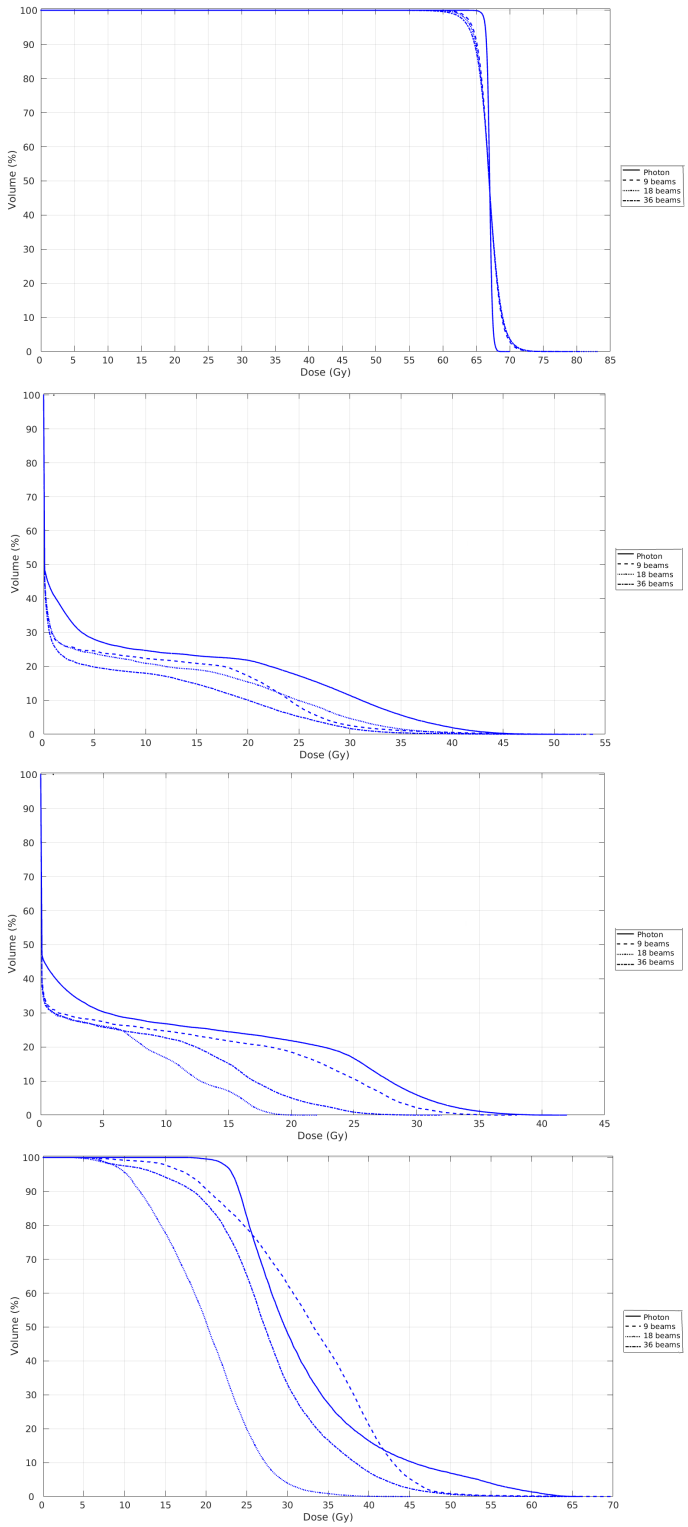

Figure 5.11: DVHs of the VMAT treatment plan and the 9, 18, and 36 beams 400 MeV VHEE treatment plans. From top to bottom, the DVHs are for the PTV, esophagus, spinal cord and plexus.

5.2.2. Comparing different energy of the electron beams

In this section the VMAT treatment plan is compared with the VHEE treatment plans for different beam energies. This is done by showing a slice of the dose distribution in the patient and showing the DVHs for different organs and the PTV.

Figure 5.12 shows a slice of the dose distribution of the 18 beam VHEE plans for different beam energies.

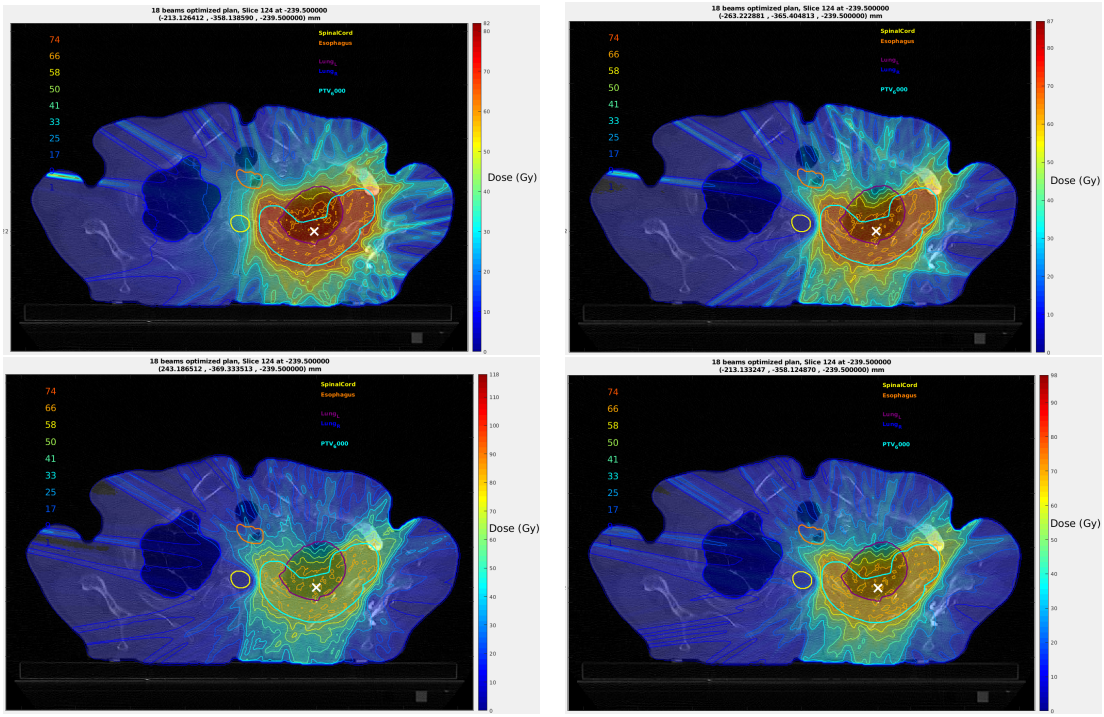

Figure 5.12: Axial slice of the dose distribution for VHEE plans with different energies. Top left is 100 MeV VHEE, top right is 200 MeV VHEE, bottom left is 300 MeV VHEE and the bottom right is 400 MeV VHEE.

In Figure 5.13 the DVHs of the PTV, esophagus, spinal cord and plexus are shown for the VMAT plan and the 18 beam VHEE plans with 100, 200, 300 and 400 MeV electron beams. The graph of the PTV is sharper for the VMAT plan than for the VHEE plans. For the esophagus the VHEE treatment plans deliver less dose to the organ than the VMAT plan. Also the higher the energy of the beam, the lower the delivered dose to the esophagus. The VHEE plans also deliver less dose to the spinal cord than the VMAT plan, but for the spinal cord the 200 MeV VHEE plan results in less dose to the organ than the higher energy VHEE plans. The DVH for the plexus shows that the higher the energy of the electron beams, the lower the dose to the plexus. Only the 400 MeV VHEE plan results in a reduction of the dose delivered to the plexus in comparison with the VMAT plan.

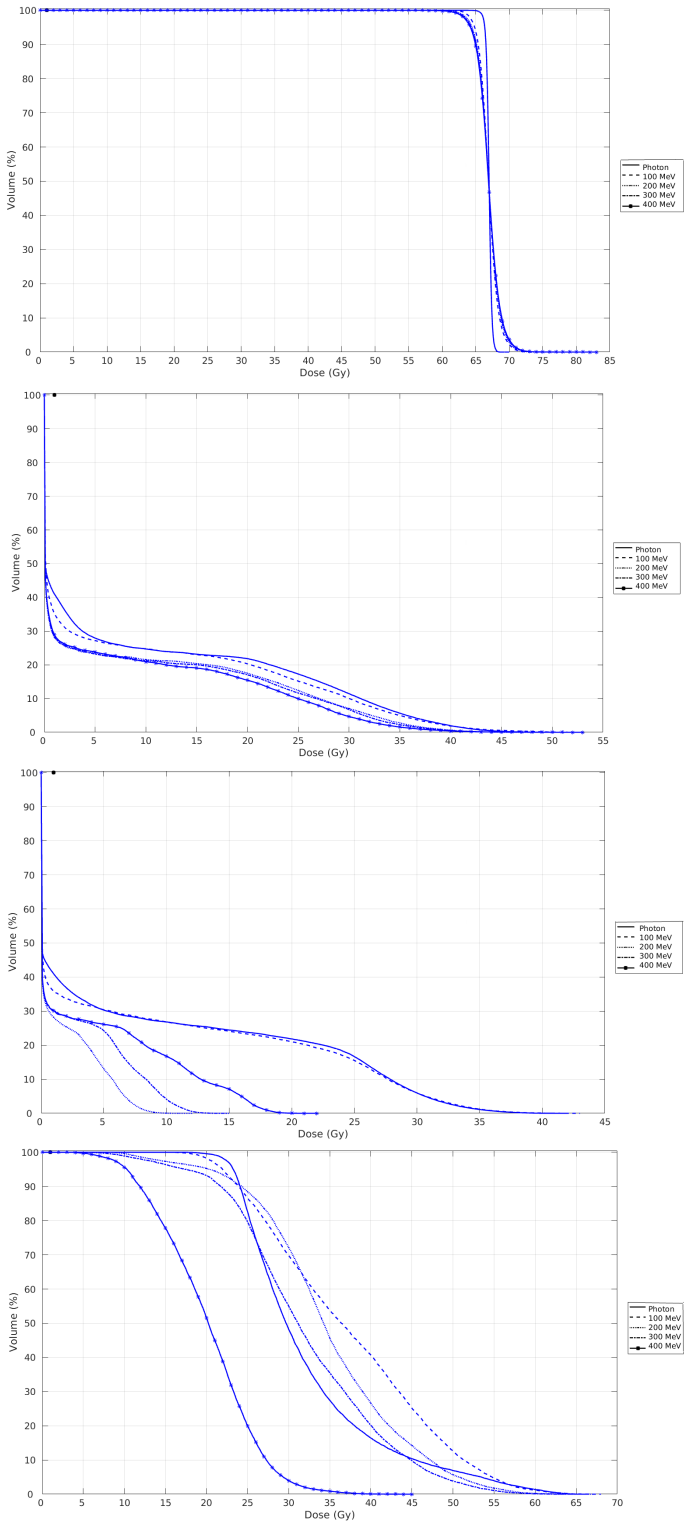

Figure 5.13: DVHs of the VMAT treatment plan and the 100,200,300 and 400 MeV VHEE treatment plans with 18 beams. From top to bottom, the DVHs are for the PTV, esophagus, spinal cord and plexus.

5.3. Computational performance

The TOPAS Monte Carlo simulations were performed on the computing cluster of Erasmus MC, called Uluru. 8 computing threads were used for each Monte Carlo simulation. The mean computing time of the simulation per beam was 19.2 ±5.6 hours. The computing time strongly depends on the number of pencil beams and the electron energy of the beams. The treatment plan optimization was also done on the Uluru cluster using 8 threads. The optimization time strongly depended on the number of beams that were used to generate the treatment plan. The optimization took on average 1.8 hours, 5.2 hours and 22.1 hours for the 9 beam, 18 beam and 36 beams treatment plan respectively.

6

Discussion

6.1. Effect of the number of beams

For the prostate cancer patients, the VHEE treatment plans delivered a lower dose to the OARs, while keeping the dose in the PTV constant, when the number of beams was increased. For the lower energies (100,200 MeV), this difference was larger than for the higher energies (300,400 MeV). By increasing the number of beams from 9 to 18 for the lung cancer patients, all the organs received less dose. However, by increasing the number of beams from 18 to 36 the esophagus received less dose, but the spinal cord and the plexus received more dose. Therefore, to determine if the 36 beam VHEE plan is beneficial in comparison of the 18 beam VHEE plan, more information is needed about the effect of these dose differences on the organs.

6.2. Effect of the beam energy

Comparing the different energy VHEE plans showed that higher energies of the electron beams, result in a reduction of the dose to the organs and an increase of the dose to the PTV. For the prostate cancer treatment all the dose metrics improved when higher energy beams were used, but the differences in these dose metrics decreased for higher energies. Therefore, it is expected that even higher energy electron beams than 400 MeV will not greatly improve the treatment plan. For the lung cancer treatment the dose to the esophagus and the plexus decrease with higher energy, but the dose to the spinal cord is lowest for the 200 MeV treatment plan. Therefore, more research needs to be done into the dose metrics to determine which electron beam energy is favorable for lung cancer treatment.

6.3. VHEE vs VMAT

For the prostate cancer patients, all the 100 MeV VHEE plans delivered a higher mean dose to the OARs than the VMAT plans. Therefore, an electron beam energy of 100 MeV is not sufficient to obtain clinically improved treatment plans in comparison with VMAT. The PTV coverage is the same for the VMAT and the VHEE plans. The CI_{riet} is significantly higher for VHEE plans with 200 MeV ($p<0.001$), 300 MeV ($p<0.001$) or 400 MeV ($p<0.001$) electron beams. The $D_{2\%}$ is significantly decreased for the 100 MeV ($p=0.011$), 200 MeV ($p=0.021$) and 300 MeV ($p=0.039$) VHEE plans. VHEE plans with at least 18 beams and at least 300 MeV electron beams, result in a reduction of all the OAR dose metrics for the prostate case, except for the left and right femoral head $D_{0.001cc}$. These differences are not statistically significant, but the differences in dose metrics were observed in every patient. From the dose metrics can be concluded that VHEE radiotherapy treatment leads to better treatment plans than clinically used VMAT for the prostate cancer patients.

For the lung cancer patients, the 18 or 36 beam VHEE treatment plans with 400 MeV electron beams result in less delivered dose to all the OARs. The 9 beam VHEE plan with 400 MeV beams reduced the dose to the esophagus and the spinal cord, but increased the dose to the plexus. From the DVHs can be seen that VHEE radiotherapy treatment can lead to better treatment plans than clinically used

VMAT for the lung cancer patients. However, more patients are needed to find a conclusion about the comparison between treatment plans of VHEE therapy and threatment plans of VMAT.

6.4. Further work

VHEE radiotherapy is a potential replacement for VMAT for treating prostate or lung cancer because the dose to healthy tissue is reduced, while the dose to the PTV is maintained. It was found that higher energy electron beams resulted in less dose to the healthy tissue. In this work the highest electron energy used was 400 MeV. Treatment plans with higher energy electron beams could result in even better healthy tissue sparing. In this work the selected number of beams were evenly spread. Better beam angle selection can lead to an improvement of the treatment plans. Before being able to treat cancer patients with VHEE radiotherapy multiple hurdles have to be overcome. The first hurdle is that the currently used generators for VHEE beams are not small enough to fit in a standard radiotherapy treatment bunker. Therefore, more progress must be made in the compact generation of VHEE beams. Secondly, the generation of the treatment plans takes too long to be used in real clinical situations. To be able to treat cancer patients with VHEE radiotherapy, a fast method has to be found to approximate the dose distribution of VHEE beams with enough accuracy for clinical use. Treatment plans could be further approved by using magnetic focusing or flash radiotherapy. With magnetic focusing the pencil beam is focused inside the PTV, which leads to a high dose in a small focal spot. Flash radiotherapy treatment uses ultra-high dose rates to the target to reduce toxicity in healthy tissue.

Bibliography

[1] The International Agency for Research on Cancer (IARC). *Global cancer observatory*. URL: https://gco.iarc.fr/.

[2] Apr. 2022. URL: https://www.wcrf.org/cancer-trends/worldwide-cancer-data/.

[3] Philip P Connell and Samuel Hellman. "Advances in radiotherapy and implications for the next century: a historical perspective". In: *Cancer research* 69.2 (2009), pp. 383–392.

[4] Jan. 2023. URL: https://www.cancercouncil.com.au/cancer-information/cancer-treatment/radiation-therapy/external-beam-radiation-therapy/.

[5] Oleksandr Maistrenko. *What is directory of Radiotherapy Centres (dirac)?* URL: https://dirac.iaea.org/.

[6] Lucy Whitmore et al. "Focused VHEE (very high energy electron) beams and dose delivery for radiotherapy applications". In: *Scientific Reports* 11.1 (2021), pp. 1–14.

[7] Ali Pashazadeh, Axel Boese, and Michael Friebe. "Radiation therapy techniques in the treatment of skin cancer: an overview of the current status and outlook". In: *Journal of Dermatological Treatment* (2019).

[8] Charles B Simone II et al. "Comparison of intensity-modulated radiotherapy, adaptive radiotherapy, proton radiotherapy, and adaptive proton radiotherapy for treatment of locally advanced head and neck cancer". In: *Radiotherapy and oncology* 101.3 (2011), pp. 376–382.

[9] Vivek Verma, Mark V Mishra, and Minesh P Mehta. "A systematic review of the cost and cost-effectiveness studies of proton radiotherapy". In: *Cancer* 122.10 (2016), pp. 1483–1501.

[10] Serena Gianfaldoni et al. "An overview on radiotherapy: from its history to its current applications in dermatology". In: *Open access Macedonian journal of medical sciences* 5.4 (2017), p. 521.

[11] *DESCRIPTION OF THE EQUIPMENT CONTAINED IN DIRAC*. URL: https://dirac.iaea.org/Home/Equipment.

[12] H Edwin Romeijn et al. "A column generation approach to radiation therapy treatment planning using aperture modulation". In: *SIAM Journal on Optimization* 15.3 (2005), pp. 838–862.

[13] Stephen Dowdell. "Pencil beam scanning proton therapy: the significance of secondary particles". In: 2011.

[14] JM Fernández-Varea, X Llovet, and F Salvat. "Cross sections for electron interactions in condensed matter". In: *Surface and Interface Analysis: An International Journal devoted to the development and application of techniques for the analysis of surfaces, interfaces and thin films* 37.11 (2005), pp. 824–832.

[15] George R Blumenthal and Robert J Gould. "Bremsstrahlung, synchrotron radiation, and compton scattering of high-energy electrons traversing dilute gases". In: *Reviews of modern Physics* 42.2 (1970), p. 237.

[16] Hooshang Nikjoo, Shuzo Uehara, and Dimitris Emfietzoglou. *Interaction of radiation with matter*. Taylor amp; Francis, 2012.

[17] M.J. Berger et al. *NIST stopping-Power amp; range tables for electrons, protons, and helium ions - SRD 124*. July 2022. URL: https://data.commerce.gov/nist-stopping-power-range-tables-electrons-protons-and-helium-ions-srd-124.

[18] James E Turner. *Atoms, radiation, and radiation protection*. John Wiley & Sons, 2008.

[19] Pankaj Tandon et al. "Interaction of Ionizing Radiation with Matter". In: *Radiation Safety Guide for Nuclear Medicine Professionals*. Springer, 2022, pp. 21–35.

[20] M.J. Berger et al. *XCOM: Photon Cross Sections Database*. Nov. 2019. URL: http://www.nist.gov/pml/data/xcom.

[21] R Teoule. “Radiation-induced DNA damage and its repair”. In: *International Journal of Radiation Biology and Related Studies in Physics, Chemistry and Medicine* 51.4 (1987), pp. 573–589.

[22] Daniel Richter. “Treatment planning for tumors with residual motion in scanned ion beam therapy”. In: (2012).

[23] JH Hendry. “Radiation biology and radiation protection”. In: *Annals of the ICRP* 41.3-4 (2012), pp. 64–71.

[24] MC Joiner. “The linear quadratic approach to fractionation”. In: *Basic clinical radiobiology* (1993), pp. 55–64.

[25] Bleddyn Jones. “Mathematical models of tumour and normal tissue response”. In: *Acta oncologica* 38.7 (1999), pp. 883–893.

[26] Marco Zaider and Leonid Hanin. “Tumor control probability in radiation treatment”. In: *Medical physics* 38.2 (2011), pp. 574–583.

[27] John T Lyman. “Complication probability as assessed from dose-volume histograms”. In: *Radiation Research* 104.2s (1985), S13–S19.

[28] Gerald J Kutcher and C Burman. “Calculation of complication probability factors for non-uniform normal tissue irradiation: The effective volume method gerald”. In: *International Journal of Radiation Oncology* Biology* Physics* 16.6 (1989), pp. 1623–1630.

[29] E. Lens. “Respiratory motion management for radiotherapy of pancreatic cancer patients”. In: 2017.

[30] Kenneth R Hogstrom and Peter R Almond. “Review of electron beam therapy physics”. In: *Physics in Medicine & Biology* 51.13 (2006), R455.

[31] EC Snively et al. “Cryogenic accelerator design for compact very high energy electron therapy”. In: *Proc. LINAC*. 2022, pp. 62–64.

[32] L Giuliano et al. “Preliminary Studies of a Compact VHEE Linear Accelerator System for FLASH Radiotherapy”. In: (2021).

[33] L Faillace et al. “Perspectives in linear accelerator for FLASH VHEE: Study of a compact C-band system”. In: *Physica Medica* 104 (2022), pp. 149–159.

[34] Maria Grazia Ronga et al. “Back to the future: very high-energy electrons (VHEEs) and their potential application in radiation therapy”. In: *Cancers* 13.19 (2021), p. 4942.

[35] Wentao Wang et al. “Free-electron lasing at 27 nanometres based on a laser wakefield accelerator”. In: *Nature* 595.7868 (2021), pp. 516–520.

[36] Kristoffer Svendsen. *Applications of Laser-Plasma Acceleration*. Atomic Physics, Department of Physics, Lund University, 2022.

[37] Lintong Ke et al. “Optimization of electron beams based on plasma-density modulation in a laser-driven wakefield accelerator”. In: *Applied Sciences* 11.6 (2021), p. 2560.

[38] Michael Litos et al. “High-efficiency acceleration of an electron beam in a plasma wakefield accelerator”. In: *Nature* 515.7525 (2014), pp. 92–95.

[39] Agnese Lagzda. *VHEE Radiotherapy Studies at CLARA and CLEAR facilities*. The University of Manchester (United Kingdom), 2019.

[40] Jasper Dijkstra. “Assessment of Very High Energy Electron therapy as a clinical modality for external beam therapy”. In: (2020).

[41] David F Kyser and NS Viswanathan. “Monte Carlo simulation of spatially distributed beams in electron-beam lithography”. In: *Journal of Vacuum Science and Technology* 12.6 (1975), pp. 1305–1308.

[42] George Dedes and Katia Parodi. “Monte Carlo simulations of particle interactions with tissue in carbon ion therapy”. In: *International Journal of Particle Therapy* 2.3 (2015), pp. 447–458.

[43] Indrin J Chetty et al. “Report of the AAPM Task Group No. 105: Issues associated with clinical implementation of Monte Carlo-based photon and electron external beam treatment planning”. In: *Medical physics* 34.12 (2007), pp. 4818–4853.

[44] Joseph Perl et al. “TOPAS: an innovative proton Monte Carlo platform for research and clinical applications”. In: *Medical physics* 39.11 (2012), pp. 6818–6837.

[45] Sea Agostinelli et al. “GEANT4—a simulation toolkit”. In: *Nuclear instruments and methods in physics research section A: Accelerators, Spectrometers, Detectors and Associated Equipment* 506.3 (2003), pp. 250–303.

[46] Sebastiaan Breedveld et al. “iCycle: Integrated, multicriterial beam angle, and profile optimization for generation of coplanar and noncoplanar IMRT plans”. In: *Medical physics* 39.2 (2012), pp. 951–963.

[47] Daniel Hyer et al. “A dynamic collimation system for penumbra reduction in spot-scanning proton therapy: Proof of concept”. In: *Medical physics* 41 (Sept. 2014), p. 091701. DOI: 10.1118/1.4837155.

[48] MMH Ragheb, JH Halton, and CW Maynard. “Minimum variance Monte Carlo importance sampling with parametric dependence”. In: *Atomkernenergie-Kerntechnik* 37 (1981), pp. 188–193.

[49] Gerrit H Jansen. “Coulomb interactions in particle beams”. In: *Nuclear Instruments and Methods in Physics Research Section A: Accelerators, Spectrometers, Detectors and Associated Equipment* 298.1-3 (1990), pp. 496–504.

[50] Jack F. Fowler. “Brief summary of radiobiological principles in fractionated radiotherapy”. In: *Seminars in Radiation Oncology* 2.1 (1992). Fractionation in Radiation Therapy, pp. 16–21. ISSN: 1053-4296. DOI: https://doi.org/10.1016/S1053-4296(05)80045-1. URL: https://www.sciencedirect.com/science/article/pii/S1053429605800451.

[51] Young Kyung Lim et al. “Microscopic gold particle-based fiducial markers for proton therapy of prostate cancer”. In: *International Journal of Radiation Oncology* Biology* Physics* 74.5 (2009), pp. 1609–1616.

[52] Marina Bakaric et al. “Experimental study of beam distortion due to fiducial markers during salvage HIFU in the prostate”. In: *Journal of therapeutic ultrasound* 6.1 (2018), pp. 1–11.

[53] Hyoung Suk Park, Yong Eun Chung, and Jin Keun Seo. “Computed tomographic beam-hardening artefacts: mathematical characterization and analysis”. In: *Philosophical Transactions of the Royal Society A: Mathematical, Physical and Engineering Sciences* 373.2043 (2015), p. 20140388.

[54] Nooshin Banaee et al. “Evaluating the effects of metal artifacts on dose distribution of the pelvic region”. In: *Journal of Cancer Research and Therapeutics* 17.2 (2021), pp. 450–454.

[55] Magdalena Bazalova-Carter et al. “Treatment planning for radiotherapy with very high-energy electron beams and comparison of VHEE and VMAT plans”. In: *Medical physics* 42.5 (2015), pp. 2615–2625.

[56] Wilfried Schneider, Thomas Bortfeld, and Wolfgang Schlegel. “Correlation between CT numbers and tissue parameters needed for Monte Carlo simulations of clinical dose distributions”. In: *Physics in Medicine & Biology* 45.2 (2000), p. 459.

[57] Tae Kyun Kim. “T test as a parametric statistic”. In: *Korean journal of anesthesiology* 68.6 (2015), pp. 540–546.